International Current Journal of Engineering and Science (ICJES)
Volume 4, Issue 11, pp 55-86, November-2025
ISSN (Online): 2583-7257
Article DOI: https://doi.org/10.47001/ICJES/2025.411010

Thickness-Dependent Structural, Morphological, Optical, and Electronic Properties of $Ge_{20}Cd_{10}Se_{70}$ Thin Films for Optoelectronic Applications

[1]Tawfik Mahmood Mohammed Ali, [2]Sarah. M. Al-Khadher, [3]*M. A. Dabban

[1]Department of Physics, Faculty of Education, University of Aden, Yemen
[2]Department of Physics, Faculty of Education-Saber, University of Aden, Yemen
[3]Department of Physics, Faculty of Science, University of Aden, Yemen
[3]Department of Health Science, Faculty of Medicine and Health Science, University of Science & Technology, Yemen
*Corresponding Author: M. A. Dabban, E-mail: dabbanm@yahoo.com

***Abstract* - In this work, the structural, morphological, optical, and electronic properties of $Ge_{20}Cd_{10}Se_{70}$ thin films were systematically investigated as a function of thickness (400-1000 nm). Energy dispersive X-ray (EDAX) analysis confirmed the stoichiometric composition and purity of the films, while X-ray diffraction (XRD) revealed the emergence of Se, $GeSe_2$, CdSe, and Cd_4GeSe_6 phases at higher thicknesses, indicating an amorphous-to-crystalline transition. SEM and AFM confirmed improved crystallinity, with crystallite size increasing (14.27 to 41.87 nm) as strain and defect density decreased. Optical measurements (200–2500 nm) showed that transmittance and reflectance varied with thickness, while both the extinction coefficient and refractive index decreased with increasing wavelength but increased with thickness. The optical band gap decreased, and the band tail width increased with thickness, consistent with Mott and Davis's model. Dispersion analysis using the Wemple–DiDomenico model indicated enhanced atomic packing, with oscillator energy decreasing and dispersion energy increasing as thickness grew. Thickness also strongly influenced dielectric constants, carrier concentration to effective mass ratio, susceptibility, nonlinear refractive index, and the electronic parameters such as plasma frequency, Penn energy, Fermi level, electronic polarizability, and molar refractivity. These results confirm that controlled thickness tailoring enables $Ge_{20}Cd_{10}Se_{70}$ thin films to exhibit tunable optoelectronic behavior, making them promising materials for optoelectronic devices.**

Keywords: Ge–Cd–Se thin films; Thickness-dependent properties; Morphological analysis; Optical band gap tuning; nonlinear optical parameters, electronic polarizability.

I. INTRODUCTION

Chalcogenide glasses have garnered significant attention due to their excellent optical properties and diverse technological applications, including infrared lasers, optical sensors, acousto-optic devices, and phase-change memory [1-6]. These materials exhibit high transmittance in the infrared region and a high refractive index (2.0–3.5), making them suitable for optical coatings and filters. Among their critical properties, crystallization behavior significantly influences thermal stability and transport mechanisms. Consequently, understanding the phase transformation kinetics in these glasses is essential for various fields, including materials science and device engineering.

Accurate characterization of optical properties in chalcogenide thin films is vital for their implementation in optical systems. The optical constants, such as refractive index and extinction coefficient are typically derived from film transmittance using techniques like Swanepoel's envelope method [7-9]. This method allows relatively precise evaluations, even without prior knowledge of film thickness and is fairly accurate with the thickness and refractive index. These characterization techniques underscore the significance of measuring optical constants to tailor materials for specific applications. Ge-Se-based materials are widely researched for their tunable structural, thermal, and optical characteristics [10-12]. The Ge-Se-Cd chalcogenide system, particularly compositions rich in selenium like $Ge_{20}Cd_{10}Se_{70}$, serves as a promising candidate for

International Current Journal of Engineering and Science (ICJES)
Volume 4, Issue 11, pp 55-86, November-2025
ISSN (Online): 2583-7257
Article DOI: https://doi.org/10.47001/ICJES/2025.411010

studying optical property variations. This system supports bulk glass formation with up to 12 at.% Cd without crystallization, allowing stable film production [13]. Thin film deposition and thickness optimization are crucial steps toward device-grade material development, motivating studies on the influence of film thickness on their overall performance.

The influence of film thickness on the structural, morphological, and optical behavior of thermally evaporated $Ge_{20}Cd_{10}Se_{70}$ thin films has not been widely reported. In this study, we present a systematic investigation into how varying thickness impacts the microstructure, linear and nonlinear optical response, dielectric constants, dispersion characteristics, and essential electronic parameters of these films. Structural and surface morphology were examined through XRD, SEM, and AFM, while EDX confirmed elemental composition. Compared with earlier work on $Ge_{15}Zn_{10}Se_{75}$ thin films [14], our research highlights the role of Cd incorporation and a higher Ge concentration (20% vs. 15%) in modifying the structural framework, bond formation, and critical electronic characteristics. Parameters such as optical susceptibility, nonlinear refractive index, plasma frequency, Penn energy, Fermi level, electronic polarizability, and molar refractivity are found to be strongly influenced by these compositional changes, which in turn provide $Ge_{20}Cd_{10}Se_{70}$ films with unique structural and optical functionalities. A further distinction of our work lies in the methodology: while AIwany et al [19] calculated optical constants using both transmittance and reflectance data, our study advances this approach by employing the Swanepoel method, which relies solely on transmittance, coupled with highly accurate thickness measurements. This methodological refinement eliminates the approximations of earlier studies, ensuring more reliable optical parameters and offering deeper insights into the optoelectronic potential of $Ge_{20}Cd_{10}Se_{70}$ thin films.

II. EXPERIMENTAL METHODS

Bulk $Ge_{20}Cd_{10}Se_{70}$ alloy were successfully synthesized by the conventional melt-quenching technique using high-purity elements 99.999% (Aldrich Chem Co., USA). Thin films of $Ge_{20}Cd_{10}Se_{70}$ with thicknesses ranging from 200–1000 nm were subsequently deposited on carefully cleaned glass substrates by thermal evaporation under high-vacuum conditions ($\approx 2\times10^{-5}$ Torr) using a high vacuum coating unit (Edwards E 306A, UK). Strict control of deposition parameters, such as substrate-source distance, deposition rate, and film thickness monitoring via quartz crystal monitor (FTM4 Edwards), ensured the homogeneity and reproducibility of the prepared thin films.

Comprehensive characterization of the prepared samples was carried out using a combination of advanced analytical techniques. Structural properties were examined by Philips X-ray diffractometer (PW 1710) with CuK_{α} radiation of wavelength 1.5418Å and Ni as a filter to analyze crystallinity, lattice parameters, and microstructural features. Surface morphology was investigated using JEOL scanning electron microscope (JSM-T200) coupled with Energy Dispersive X-ray (EDX) spectroscopy for elemental composition, and Atomic Force Microscopy (AFM)-SPM-AA5000 contact mode Augestrom Advanced Inc., 2008, USA- for three-dimensional surface topography and roughness evaluation. Optical properties, including transmission, reflection, absorption, and band gap, were measured over a broad spectral range using a LAMBDA 750 UV/Vis/NIR spectrophotometer. These combined experimental approaches provided a detailed understanding of the structural, electrical, and optical behaviour of the $Ge_{20}Cd_{10}Se_{70}$ alloys and thin films, forming a reliable basis for correlating thickness-dependent properties with potential optoelectronic applications.

III. RESULTS AND DISCUSSION

3.1 XRD structural analysis and EDX confirmation

A map of the distribution of the component elements of the $Ge_{20}Cd_{10}Se_{70}$ film with thickness of 400 nm was obtained through counting-energy routes using the dispersive approach with X-energy (EDX) as shown in **Fig.1.** EDX analysis indicates that the ratio of constituent elements is nearly identical to the supposed composition, and strange elements will not be detected. XRD patterns of the as-prepared $Ge_{20}Cd_{10}Se_{70}$ films with various thicknesses are displays in **Fig.2 (a-d)**. The fully amorphous structure of the film with 200 nm thickness is illustrated in **Fig. 2(a)**. The crystallinity pathways of the investigated films grow with increasing film thickness, as seen in **Fig.2 (b-d)**. Crystallization revealed the formation of certain peaks, indicating a polycrystalline nature. The XRD findings of $Ge_{20}Cd_{10}Se_{70}$ films at various thicknesses demonstrate the presence of highly

International Current Journal of Engineering and Science (ICJES)
Volume 4, Issue 11, pp 55-86, November-2025
ISSN (Online): 2583-7257
Article DOI: https://doi.org/10.47001/ICJES/2025.411010

crystalline Se, $GeSe_2$, and CdSe phases as well as the triple Cd_4GeSe_6 phase after increasing the film thickness to 1000 nm, which is in accordance with the JCPDS patterns listed in Table 1. Slight shifts in the peak positions in the 2θ scan is common due to residual stresses, substrate-induced strain, or compositional changes in the film [15]. As a result, the crystallinity of $Ge_{20}Cd_{10}Se_{70}$ films improves with increasing film thickness as the degree of disorder and defects decreases. Hence, it is predicted that the $Ge_{20}Cd_{10}Se_{70}$ films will crystallize more readily as film thickness increases due to a decrease in the degree of disorder and internal defects. The average crystallite size (D), internal lattice microstrain (ε), dislocation density (δ), and number of crystallites (N) of the crystalline films as a result of the crystallization process with increasing thickness were calculated to verify the accuracy of these predictions. Many attempts reported to separate and evaluate the size and strain parameters from the occurring line broadening such as the Variance method, Warren-Averbach method, and Williamson-Hall (W-H) analysis among them, W-H method is a simplified approach to deconvolute strain and finite size induced broadening. Williamson-Hall analysis of the XRD data was used to determine both the residual strain and the coherent crystal size [16]. In the W–H approach, the crystallite size (Depye-Scherrer considerations $D=K\lambda/\beta_{hkl}\cos\theta$) and strain effects (Stokes-Wilson equation $\varepsilon= \beta_{hkl}/\tan\theta$ [17,18]. The former varies with respect to 1/cosθ and the latter varies with respect to tan θ, related broadening as the following equation:

$$\left.\begin{aligned} \beta_{hkl} &= \beta_D + \beta_\varepsilon \\ \beta_{hkl} &= \frac{0.94\lambda}{D\cos\theta_{hkl}} + 4\varepsilon\tan\theta_{hkl} \\ \frac{\beta_{hkl}\cos\theta_{hkl}}{\lambda} &= \frac{0.94}{D} + \frac{4\varepsilon\sin\theta_{hkl}}{\lambda} \end{aligned}\right\} \quad (1)$$

Where β_{hkl} is the full width at half maximum (FWHM) of the XRD peaks, D is the crystallite size, ε is the lattice micro-strain, λ is the X-ray wavelength, and θ is the Bragg angle. The plot of (βr cosθ)/λ vs. (sinθ)/λ must be straight lines as shown in **Fig. 3**.The slope of these plots indicates residual microstrain, and the reciprocal of the intercept gives average crystallite size. The crystallite size and strain values of each film were estimated and tabulated in **Table 2**. With an increase in film thickness from 400 to 1000 nm, the crystalline size increases from 14.27 to 41.87 nm, while the micro-strain decreases. Understanding the optical properties of these films depends on the thickness dependences of the residual strain and crystallite size. Furthermore, a dislocation is an imperfection in a crystal, and the dislocation density (δ) is the density of defects or the length of dislocation lines per unit volume of the crystal, which can be determined using Williamson and Smallman's formula: $\delta=1/D^2$ [19]. The number of crystallites per unit surface area N may also be computed using the relation: $N=d/D^3$ **[69],** where d is the thickness of the films. In polycrystalline films, dislocated atoms occupy the regions near the grain boundary. Generally the dislocation density and number of crystallites per unit surface area are inversely proportional to crystalline size so it were observed that δ and N values decreased with increase in film thickness as shown in **Table 2.**

3.2 Morphological study

Further evidence for the structural transformation from amorphous to crystalline state was investigated for the studied thin films. The morphology of as-prepared $Ge_{20}Cd_{10}Se_{70}$ thin films of different thicknesses have been characterized by the scanning electron microscope, SEM, as shown in **Fig. 4 (a-d)**. For the thinnest (200 nm) film (**Fig. 4 a**), regularly shaped nanoflakes-like structures of small sizes dispersed at cross-linking chains with the existence of short-range order were distributed on the amorphous background. Nanoflakes that were bigger and more densely stacked as a result of increasing film thickness are shown in **Fig. (b-c)**. With further increase in the thickness of the film (up to 1000 nm), the nanoflakes changed into grains of irregular forms (**Fig. 4 d**). The improved crystallinity of films with increased thickness is confirmed by these photographs. By comparing **Fig. 2 and Fig. 4**, it is clear that there is excellent agreement between the SEM observations and the X-ray patterns. The change in morphology with thickness is also observed in other chalcogenide thin film [**20**]. The microstructure and thickness of $Ge_{20}Cd_{10}Se_{70}$ film on glass substrates were determined using a SEM cross-sectional views as

International Current Journal of Engineering and Science (ICJES)
Volume 4, Issue 11, pp 55-86, November-2025
ISSN (Online): 2583-7257
Article DOI: https://doi.org/10.47001/ICJES/2025.411010

observed by a SEM are shown in **Fig. 5 (a-d)**. Images reveal that the films are smooth, without of cracks or pores. The findings of measuring the thickness using an electron microscope, which are shown in the figure, confirmed that there is a very minor variation in the thickness of the films and that their average values are extremely near to those that were previously assumed or computed optically, as we'll discover later.

To more understand the surface features, quality, and size distribution of the deposited GeSe films, AFM analysis was performed using an atomic force microscope in tapping mode under ambient conditions. The two dimensional, (2D, and three dimensional (3D) topography images of $Ge_{20}Cd_{10}Se_{70}$ films with thicknesses of 200, 400, 800 nm and 1000 nm prepared by thermal evaporation technique are shown in **Fig. 6**. Roughness (R_a) and root mean square (RMS) roughness (R_q) and average grain size were determined by AFM images within the scanned area (3.5 μm × 3.5 μm) using **Nonoscope v720** imaging software. The surface morphology reveals the nano-crystalline uniform grains distribution which combine to make denser films significantly with the increased thickness. It is observed from the images that the surface of the films exhibited ascertain degree of roughness, and the film becomes rougher with increasing thickness. Roughness (Ra) and root mean square (RMS) roughness (Rq) values were estimated and listed in **Table 3**. This result indicates that the growth of larger grains leads to an increase in surface roughness with increasing thickness. These results are comparable to those reported in previous studies for various chalcogenide thin films with increasing film thickness. [21-23]. To confirm these hypotheses, **Fig. 7** shows a distribution histogram of the percentage of $Ge_{20}Cd_{10}Se_{70}$ films of different thicknesses as a function of grain diameter. It can be clearly seen from the figure that the average grain size is (4.18, 16.5, 32.2, and 72.1) nm for the film thicknesses of (200, 400, 800, and 1000) nm, respectively. **Table 3** clearly shows that the root mean square of surface roughness increases with different thickness means delivering of more energy implies a high polycrystalline [24]. Because the AFM measurement directly visualizes the grains, the average grain size values (given in **Table 3**) disagree with those estimated by XRD. The nano structural and phase transitions that occur in the investigated films as the thickness of the film increases allow us to use them in many novel applications, such as optoelectronic devices.

3.3 Optical properties

3.3.1 Interference fringes in transmission and reflection spectra

Usually, the optical characteristics and parameters of any material are strongly dependent upon the interactions between the incident light waves and that material. In the present work, the optical properties have studied in term of the transmission T_λ, and reflection, R_λ spectra, measured in a broad spectral range from 200 to 2500 nm, which have shown in **Fig. 8 (a and b)**. It is observed that the interference fringes are more visible as the film thickness increases. Interference fringes are produced due to reflection and transmission of the incident wave between film-air, film-substrate and substrate-air interfaces. Furthermore, the absorption edge shifts towards higher wavelength with increasing the film thickness. This could be attributed to the changes occurred in the structural properties of the films as result of the effect of the film thickness. In addition, due to the inhomogeneity of some parts of the film surface, there are also differences in the depth of interference fringes in the spectrum. In the UV region, the transmittance is nearly non-existent, but it rapidly increases in the VIS-NIR region, reaching about 0.95 % for all films. Thin films can be employed in modern applications such as the thermal control of window coatings for cold environments and also for anti-reflective coatings due to their high transmittance in the VIS-NIR ranges.

3.3.2 Evaluation of the film thickness and refractive index

The optical constants are the real and imaginary parts of the complex refraction index $\tilde{n} = n + k_{ex}$. The real part represents the refractive index (n), while the imaginary part represents the absorption (extinction coefficient). The refractive index of a material reflects the ratio of the speed of light in a vacuum to its speed in the medium. It is an important parameter, which is an essential property for the practical applications. It is associated with the electronic polarizability of ions as well as electric field within the material. An increase in the refractive index indicates that the polarization of the medium is increasing. The refractive index (n) and thickness of the films (d) were determined from transmission spectra using Swanepoel's envelope method, which applies upper and lower transmittance envelopes formed by interference fringes [25]. Both the upper and lower envelopes for all studied films were computer-generated using the **Envelope.exe** program as shown in **Fig. 9**. The values of

International Current Journal of Engineering and Science (ICJES)
Volume 4, Issue 11, pp 55-86, November-2025
ISSN (Online): 2583-7257
Article DOI: https://doi.org/10.47001/ICJES/2025.411010

film thickness are listed in **Table 4**. One notes that the calculated thickness values deviate slightly from the expected values due to the small perturbation of the holder rotation during evaporation, the difference in the depth of the interference fringes in the spectra and the side view of the scanning SEM records. The spectral of the refractive index, *n*, for $Ge_{20}Cd_{10}Se_{70}$ films is shown in **Fig. 10**. All films exhibit a normal dispersion, where the refractive index, n, decreases as the wavelength increases. The gradual decrease of the refractive indexes with increasing wavelength means the efficient transmittance of IR, and visible light; therefore, such materials are suggested to be used for plating the building materials for heating usage. It was also seen that the values of the refractive index increases with increasing film thickness. It can be seen that the refractive index increases with film thickness. The refractive index is related to the density and polarizability of the chalcogenide material. Therefore, changing the film thickness can change the density and/or polarizability of $Ge_{20}Cd_{10}Se_{70}$ films. Similar behaviour was previously reported by Shaaban et.al [26]. Furthermore, the refractive index (n) values can be fitted to a suitable function, such as the two-term Cauchy dispersion relation, which also allows extrapolation to shorter wavelengths [27].The values of a, and b for $Ge_{20}Cd_{10}Se_{70}$ films are listed in **Table 4**.

$$n = a + \frac{b}{\lambda^2} \tag{2}$$

3.3.3 Dispersion parameters and high dielectric constants analysis

Dispersion is a significant factor in the development of optical communications and spectrally dispersive devices; hence it plays an important role in the research of optical materials [28]. In addition, determination of the dispersion energy plays a major role in determining the behavior of the refractive indices and properly normalizes the interaction potential describing these optical effects which is due to the relationship between the electronic and optical properties of the material and its chemical bonds. Therefore, this topic needs to be discussed in detail to study the effect of film thickness on dispersion parameters of the refractive index of $Ge_{20}Cd_{10}Se_{70}$ films. The best model available to study these parameters is the single effective oscillator model proposed by Wemple-Di-Domenico, WDD. This model successfully examines the effective individual oscillator energy (E_o) and dispersion or intensity energy (E_d), determining their values with very accurate results. Therefore, according to the WDD dispersion model, the refractive index n is related to these energies (E_o and E_d) by the following expressions [29,30]:

$$n^2 - 1 = \frac{E_d E_o}{{E_o}^2 - (h\nu)^2} \tag{3}$$

Rearranging this equation to get:

$$(n^2 - 1)^{-1} = \frac{{E_o}^2 - (h\nu)^2}{E_d E_o} = \frac{E_o}{E_d} - \frac{(h\nu)^2}{E_o E_d} \tag{4}$$

where E_o is the oscillator energy and considered as an average energy gap (The physical meaning of E_o is that it stimulates all the electronic excitation involved and take values near the main peak of the imaginary part of the dielectric constant spectrum), and E_d is the dispersion energy which measures the average strength of the interband optical transitions and is related to the chemical bonding and the charge distribution within each unit cell. For the diamagnetic chalcogenides glasses, such as our current case, **Eq. 4** could be rewritten as [31]:

$$(n^2 - 1)^{-1} = \left(\frac{\hat{E}_o}{\hat{E}_d} - \frac{(h\nu)^2}{\hat{E}_o \hat{E}_d} \right) + \left(\frac{E_o}{E_d} - \frac{(h\nu)^2}{E_o E_d} \right) \tag{5}$$

International Current Journal of Engineering and Science (ICJES)
Volume 4, Issue 11, pp 55-86, November-2025
ISSN (Online): 2583-7257
Article DOI: https://doi.org/10.47001/ICJES/2025.411010

Here $\hat{E}_o$ and $\hat{E}_d$ express for the transition from *f* to *d* level but E_o and E_d calculate for the transition from *s* and/or *p* to d level. **Fig. 11**, illustrates the plot of $(n^2-1)^{-1}$ versus $(h\upsilon)^2$ for the investigated films, which yields a straight line for normal behavior having the slope $(E_oE_d)^{-1}$ and the intercept with the vertical axis is E_o/E_d from which E_o and E_d in the high energy region, and also $\hat{E}_o$ and $\hat{E}_d$ in the low energy region can be easily obtained for $Ge_{20}Cd_{10}Se_{70}$ films from **Eq. 5**. The estimated values of E_o and E_d of our samples are listed in **Table 5**. The deviation from linearity at a longer wavelength for the curves in **Fig. 11** is usually observed due to the negative contribution of lattice vibrations on the refractive index [32]. It is observed that the values of $\hat{E}_o$ and E_o decrease, while $\hat{E}_d$ and E_d increases with increasing film thickness. The increase of the values of $\hat{E}_d$ and E_d as a function of the film thickness could be attributed to the change in the atoms diffusion rate in the investigated films, indicating an increase of the number of atoms at interstitial cites [33]. The reduction in oscillator energy is associated with the decrease in energy band gap (Tauc energy), i.e. the greater the lattice oscillator energy, the greater the optical band gap [26]. This is not surprising, as the energy of the oscillators is usually believed to be the overall energy of the material. It is evident from **Table 5** that the average ratio of $E_o/E_g \approx 2$, which is in good agreement with that mentioned by Tanaka [34,35]. The static refraction index , n_o, and the high dielectric constant, ε_∞ at $h\upsilon \to 0$ in low and high energy regions for the $Ge_{20}Cd_{10}Se_{70}$ films can also be calculated by using the two energy values E_d and E_o, which were derived from **Fig.11** based on the single effective oscillator model as follows [36]:

$$\left.\begin{aligned} \hat{n}_0 &= \sqrt{1+\frac{\hat{E}_d}{\hat{E}_o}} \quad and \quad \hat{\varepsilon}_\infty \approx \hat{n}_o^2 = 1+\frac{\hat{E}_d}{\hat{E}_o} \\ n_0 &= \sqrt{1+\frac{E_d}{E_o}} \quad and \quad \varepsilon_\infty \approx n_0^2 = 1+\frac{E_d}{E_o} \end{aligned}\right\} \tag{6}$$

The obtained values of the static refraction index, n_o, and the high dielectric constant, ε_∞ were estimated and listed in **Table 5**. It is clear that the values of these two optical parameters increase with increasing of film thickness.

Drude's theory is used to calculate the lattice dielectric constant, (ε_L) for the $Ge_{20}Cd_{10}Se_{70}$ films at different thickness, which includes the contributions of free carriers and lattice vibration modes of dispersion as follows [37]:

$$n^2 = \varepsilon_L - \left(\frac{e^2 N}{4\pi^2 c^2 \varepsilon_o m^*}\right)\lambda^2 \tag{7}$$

where *e* is the electronic charge, *c* is the light velocity, ε_o is the free space dielectric constant (8.845×10^{-12} F/m), *N* and m^* are the free carrier concentration and its effective mass respectively. To verify **Eq. 7**, the plots of n^2 versus λ^2 of $Ge_{20}Cd_{10}Se_{70}$ films at different thicknesses are shown in **Fig. 12.** For each film thickness, ε_L and N/m* values were determined from the slopes and intercepts of the fitted lines in **Fig. 12** and listed in **Table 6**. As film thickness increases, both ε_L and N/m* change in the same manner, which can be attributed to a change in the carrier concentration N since the effective mass m is constant. This may be explained by the increased scattering of free carriers by ionized impurities and defects [38,39].

The plasma resonance frequency, ω_p (a resonance frequency at which electrons freely oscillates around their equilibrium position) can be expressed as [40, 41]:

$$\omega_p = (e^2 N / \varepsilon_o . \varepsilon_{\infty(1)} . m^*)^{1/2} \tag{8}$$

International Current Journal of Engineering and Science (ICJES)
Volume 4, Issue 11, pp 55-86, November-2025
ISSN (Online): 2583-7257
Article DOI: https://doi.org/10.47001/ICJES/2025.411010

Depending on the computed values of N/m^* and ε_L, the plasma resonance frequency ω_p can be calculated and listed in **Table 6.** The behavior of plasma frequency ω_p can be reflected by the corresponding change in $\left[(N/m*)/\varepsilon_L\right]^{1/2}$.

3.3.4 Estimation of Sellmeier parameters

The refractive index (n) at low frequencies has been found to obey the classical dispersion relation of the single-oscillator model proposed by Sellmeier, given by [42,43]:

$$(n^2-1)^{-1}=\frac{1}{S_o\lambda_o^{\ 2}}-\frac{1}{S_o}\lambda^{-2} \tag{9}$$

where S_o is the average oscillator strength ($S_o=(n_o^2-1)/\lambda_o^2=E_d/E_o\lambda^2{}_o$) and λ_o is the oscillator wavelength (λ_o= hc/E_o). Based on the previously determined values of E_o and E_d the parameters S_o, and λ_o can be easily calculated and listed in **Table 6**. It can observe that both values of S_o, and λ_o increased as film thickness increased However, the E_o/S_o ratio is of the same order as that obtained by Wemple and Di-Domenico for some materials with several crystal structures. (10^{-14} eV.m^2) [44].

3.3.5 Extraction of Absorption coefficient, Optical band gap and Urbach energy

The absorbance $x(\lambda)$ for the region of strong absorption where the interference maxima and minima converge to a single curve can be computed using the Connell and Lewis method [45]:

$$x(\lambda)=\frac{p+[P^2+2QT_\alpha(1-R_2R_3)]^{1/2}}{Q} \tag{10}$$

where P=(R_1-1) (R_2-1) (R_3-1), Q=2Tα_{opt} (R_1R_2+ R_1R_3- 2$R_1R_2R_3$), R_1 is the reflectance of the air-film interface (R_1=[(1-n)/(1+n)]^2), R_2 is the reflectance of the film-substrate interface (R_2=[(n-s)/(n+s)]^2), and R_3 is the reflectance of the substrate-air interface (R_3=[(s-1)/(s+1)]^2). The relationship $x(\lambda)=\exp(-\alpha_{opt}d)$ can also be solved to determine the values of the absorption coefficient (α_{opt}) because films thickness (d) is already known. The absorption coefficient (α_{opt}) is defined as a measure of the percentage of loss in light from the falling beam directly at a given thickness. **Fig. 13** shows the dependence of the absorption coefficient (α) on the incident photon energy of the $Ge_{20}Cd_{10}Se_{70}$ films. The absorption edge shifts towards lower photon energies with increasing film thickness, indicating that the optical band gap is affected by thickness. The absorption spectra can also be divided into two regions based on **Fig. 13** the low absorption region ($\alpha< 10^4$ cm^{-1}) and the high absorption region ($\alpha \geq 10^4$ cm^{-1}).

At region ($\alpha< 10^4$ cm^{-1}) that gives more information about the localized states in the band structure, the absorption coefficient (α) varies exponentially with photon energy and follows Urbach's relation [46]:

$$\alpha(\nu)=\alpha_o\exp(h\nu/E_U) \tag{11}$$

The inverse of the slope of the line that results from plotting ln(α_{opt}) vs hν, shown in **Fig. 14** should equal Urbach energy, E_U which is the width of the localized states. The calculated E_U values for different films are records in **Table 7**.

Higher absorption coefficient values, $\alpha \geq 10^4$ cm^{-1}, correspond to transitions between extended states in both the valence and conduction bands, where the Tauc relation's behavior is valid [47]:

International Current Journal of Engineering and Science (ICJES)
Volume 4, Issue 11, pp 55-86, November-2025
ISSN (Online): 2583-7257
Article DOI: https://doi.org/10.47001/ICJES/2025.411010

$$(\alpha h\nu) = A(h\nu - E_g)^r \quad (12)$$

where *r* takes the value 1/2 for a direct allowed transition, the value 3/2 for a direct forbidden transition, and the values 2 and 3 for an indirect allowed and an indirect forbidden transition, respectively. A is constant dependent on the transition probability and E_g^{opt} is the specimen's optical band gap. Therefore, to know the type of the probable electronic transition, anyone must try to graphically represent ($\alpha_{opt}h\nu$) versus ($h\nu$) four times. Since the value of the power factor (r=1/2, 2, 3/2, and 3) should change each time, the graph with the longest straight line represents the type of electrical transition, i.e. it produces the desired result. It should be noted that in most cases of the semiconducting crystalline materials (but not all) the electronic transmission is an allowed direct transition, while for semiconducting amorphous materials; it is probable to be an allowed indirect transition. But, it is not a rule, where there are some materials are known to be direct and indirect semiconductors [48,49]. Plotting $(\alpha_{opt}h\nu)^{0.5}$ and $(\alpha_{opt}h\nu)^2$ versus the photon energy ($h\nu$) of the incident radiation at the absorption edge allowed us to calculate the values E_g^{ind} and E_g^d of $Ge_{20}Cd_{10}Se_{70}$ films at various thicknesses using the intercept of straight lines at $(\alpha_{opt}h\nu)^r = 0$, as shown in **Fig. 15 (a and b)**. For all films, there were two distinct linear parts indicating the existence of both indirect and direct optical transitions. Extrapolating the straight parts of the two relations towards lower photon energies yields values of the optical band gaps. The obtained values of E_g^{ind}, E_g^d and E_U are summarized in **Table 7** and replotted in **Fig.16**. The optical band gap values obtained are consistent with the absorption edge, confirming the reliability of the measurements. With increasing film thickness, E_g decreases as the absorption coefficient α shifts to lower energies. This variation in E_g and E_u follows the Mott–Davis model, which predicts an inverse relation between these parameters in amorphous and partially crystalline semiconductors. [50]. The number of unsaturated bonds or dangling bonds surrounding the surface of the crystallites increased with the film thickness, leading to the creation of localized states in the band states and a reduction in the optical energy gap of the investigated films [51-55].

3.3.6 Estimation of extinction coefficient

Fig. 17 shows the dependence of the extinction coefficient *k* of $Ge_{20}Cd_{10}Se_{70}$thin films at different film thickness on the wavelength λ, based on the equation $k_{ex} = \alpha\lambda/4\pi$. The first observation in **Fig. 17** is that k_{ex} reduces with increasing wavelength and increases with increasing film thickness. Light scattering and a decrease in absorbance are essential for the extinction coefficient decreasing as wavelength increases, whereas an increase in the extinction coefficient with an increase in film thickness is caused by an increase in the free carrier concentration with increasing film thickness [56].

3.3.7 Electrical susceptibility

Electrical susceptibility (χ_c) is defined as a dimensionless, proportional parameter that describes the degree of polarization of a dielectric material in response to an applied electric field. The higher the electrical sensitivity means the higher the material's ability to respond to electric field polarization, thereby minimizing the overall electric field in the material. It is in this way that the electric susceptibility affects the electric permittivity of the material and thus affects several other phenomena such as the capacitance of capacitors to the speed of light. *etc*. One can obtain the electrical susceptibility from the two optical constants, n and k as follows [57]:

$$\chi_c = \frac{1}{4\pi}\left[n^2 - k_{ex}^2 - \varepsilon_\infty\right] = \frac{1}{4\pi}\left[\varepsilon_r - \varepsilon_\infty\right] \quad (13)$$

International Current Journal of Engineering and Science (ICJES)
Volume 4, Issue 11, pp 55-86, November-2025
ISSN (Online): 2583-7257
Article DOI: https://doi.org/10.47001/ICJES/2025.411010

Where ε_r is the real dielectric constant which previously mentioned. The electrical susceptibility, χ_c of the studied thin films in terms of the photon energy, is offered in **Fig. 18**. The electrical susceptibility increases with increasing photon energy and the film thickness. Consequently, the studied thin films can polarize in the electric field.

3.3.8 Non-linear refractive index (Kerr effect)

Nonlinear influences are seen when high-intensity light moves across a matter. The easiest of these are the Kerr impacts, which represent the difference in the refractive index as being to the optical intensity, I, namely, $(\Delta n = n_2 \times I)$. The non-linear refractive index is strongly depending on incident intensity. If the substance is subjected to the strong electrical field of the incident light, the polarization is no longer equal to the electrical field, and the polarization variance must be increased with the square of the electrical field [58]. The nonlinear refractive index is obtained from the Tichy and Ticha relationship, which is a synthesis of Miller`s popularized rule and the static refractive index extracted from the WDD pattern [33].

$$n_2\,(esu.eV^4) = \left[\frac{12\pi}{n_o}\right]\chi^{(3)} \tag{14}$$

Where $\chi^{(3)}$ is third-order non-linear susceptibility which is obtained from the following equation [59];

$$\chi^{(3)}\,(esu) = 1.7\times10^{-10}\left[\chi^{(1)}\right]^4 \tag{15}$$

where χ(1) is linear susceptibility is expressed as:

$$\chi^{(1)} = \frac{1}{4\pi}\left[\frac{E_d}{E_o}\right] \tag{16}$$

Therefore, χ(3) is expressed as

$$\chi^{(3)}\ (esu) = \frac{1.7\times10^{-10}}{16\pi^4}\left[n_o^2-1\right]^4 = 6.82\times10^{-15}\left(\frac{E_d}{E_o}\right)^4 \tag{17}$$

The values of the linear first-order susceptibility, $\chi^{(1)}$ and the nonlinear third-order susceptibility, $\chi^{(3)}$ are listed in **Table 8**. From this table, it is found that the values of these quantities increase with increasing the film thickness. In addition, according to a semi-empirical equation suggested by Boling et al. for forecasting the second-order refractive index, n_2 from the linear refractive index, n for semiconductors, takes the simplest form [60, 61]:

$$\left.\begin{aligned} n_2(\times10^{-13}\,esu) &= 391\frac{(n-1)}{\upsilon_d^{5/4}} \\ &Here, \\ \upsilon_d &= \frac{n_{(\lambda=589\,nm)}-1}{n_{(\lambda=486.1nm)}-n_{(\lambda=656.3nm)}} \end{aligned}\right\} \tag{18}$$

International Current Journal of Engineering and Science (ICJES)
Volume 4, Issue 11, pp 55-86, November-2025
ISSN (Online): 2583-7257
Article DOI: https://doi.org/10.47001/ICJES/2025.411010

According to both of **Eqs 15 and 16,** the obtained values of $\chi^{(3)}$ and n_2 versus λ is offered in **Fig. 19** and **Fig. 20**, respectively. From this, one can notice that the both parameters increases with increasing film thickness and decreases with increasing the wavelength, λ. The nonlinear refractive index, n_2 is increasing, as the linear refractive index, and for the same reasons mentioned above.

3.3.9 Electronic properties

3.3.9.1 Energies of Plasmon, Penn and Fermi

The importance of electronic parameters of optical materials lies in their employment in various fields of application, which include, for example, the field of solar cells, optical sensors, detectors, diodes, optical filters, display screens, alarm devices, photoelectric circuits, and so on. After knowing the plasma frequency, ω_p an important set of parameters can be easily extracted, called electronic parameters, and they include Plasmon, Penn, and Fermi energies, (Ψ , E_p and E_F) which are computed according to the following equations [62,63]:

$$\left.\begin{aligned} \Psi &= \hbar\omega_p = (h/2\pi).\omega_p \\ E_P &= \Psi \Big/ \sqrt{(\varepsilon_\infty - 1)} \\ E_F &= 0.3\times\sqrt[3]{\Psi^4} \end{aligned}\right\} \quad (19)$$

Where $\hbar = (4.135\times10^{-15}/2\pi)\left(\frac{eV}{s}\right)$. In the related side, the total effective count of valence electrons n_{eff} is extracted according the following [60]:

$$\left.\begin{aligned} n_{eff} &= 0.12056\ (\Psi^2\times V_m),\quad where\quad V_m = \frac{M}{\rho} \\ M &= \left(\frac{(20\times M_{Ge})+(10\times M_{Cd})+(70\times M_{Se})}{100}\right) \\ \rho &= \left(\frac{(20\times \rho_{Ge})+(10\times \rho_{Cd})+(70\times \rho_{Se})}{100}\right) \end{aligned}\right\} \quad (20)$$

Here, V_m incarnates the molar volume, ρ portrays the density of studied composition (with unit of g/cm^3) and M represents the molecular weight (with unit of g/mol.). The values of energies of Plasmon Ψ , Penn E_p , and Fermi E_F as well as the number of active electrons n_{eff} are recorded in **Table 8**. These values increase with thickness up to 500 nm and then almost remain constant after that. A plasma resonance frequency that is closely related to these quantities is the main cause of the observed behavior in these quantities.

3.3.9.2 The electronic polarizability of thin films

Thin films' electronic polarizability is the second path that should be known in electronic parameters as it is useful in various optoelectronic applications. Polarization is thought to be the primary cause of wave generation in glasses during electronic processes. Internal charge transfer allows the electron gas cloud to migrate farther away from the nucleus, resulting

International Current Journal of Engineering and Science (ICJES)
Volume 4, Issue 11, pp 55-86, November-2025
ISSN (Online): 2583-7257
Article DOI: https://doi.org/10.47001/ICJES/2025.411010

in a net dipole moment. Mechanical forces must form the non-linear equations for the efficient displacement. Continuous attention was paid to improving the computation of polarization in solids due to their wide range of applications. The electronic polarization α_p in terms of the three mentioned energies is computed from the following formula [64,65]:

$$\alpha_p = (0.4\times10^{-24}).\left(\frac{(\Psi)^2.[1-(\frac{E_P}{4E_F})+\frac{1}{3}(\frac{E_P}{4E_F})^2]}{(\Psi)^2[1-(\frac{E_P}{4E_F})+\frac{1}{3}(\frac{E_P}{4E_F})^2]+3E_P^2}\right)\times V_m \quad (21)$$

Reddy et al. [66] proposed the following empirical formulas to extract the electronic polarization in terms of the optical band gap:

$$\alpha_p = \left(0.4\times10^{-24}\right).\left(\frac{(12.41-\sqrt{E_g-0.365})}{(12.41+2\sqrt{E_g-0.365})}\right)\times V_m \quad (22)$$

$$\alpha_p = 0.4\times10^{-24}\left(\frac{(5.563-\left[0.033\times168.58+30.3\ln(0.027E_g)\right])^2-1}{(5.563-\left[0.033\times168.58+30.3\ln(0.027E_g)\right])^2+2}\right)\times V_m \quad (23)$$

$$\alpha_p = (0.4\times10^{-24})\times\left(\frac{4.06-\sqrt{E_g}}{4.06}\right)\times V_m \quad (24)$$

In terms of ε_∞, α_p is computed based on the Clausius-Mossotti Model (CMM) as follows [67,68]:

$$\alpha_p = \left(0.4\times10^{-24}\right)\times\left(\frac{(\varepsilon_\infty-1)}{(\varepsilon_\infty+2)}\right)\times V_m \quad (25)$$

The values of α_P are calculated and listed in **Table 9**. Values of α_P increase as film thickness increases, which may be explained by the fact that the refractive index of the films noticeably rises as they thicken due to the increase in scattering angles within the material's lattice matrix.

3.3.9.3 Molar refractivity

The molar refractivity, R_m is a function of a material's overall polarizability; it relies on the static refractive index in the low and high region according to the equation of Lorentz-Lorentz. Hence, for the material under investigation, R_m is computed as [69]:

$$R_m = \left[\frac{(n_0^2-1)}{(n_0^2+2)}\right]\times V_m \quad (26)$$

The computed values of R_m in the low and high regions are calculated and listed in **Table 9**. Ones observed that the increase of R_m with increasing film thickness because of the increasing both of the static refractive index and the molar volume.

International Current Journal of Engineering and Science (ICJES)
Volume 4, Issue 11, pp 55-86, November-2025
ISSN (Online): 2583-7257
Article DOI: https://doi.org/10.47001/ICJES/2025.411010

3.3.9.4 Refractive index- energy gap dependence

The refractive index and the energy gap of the semiconductors are two fundamental physical features that describe their optical and electronic properties. In this context, so several empirical equations correlate between the refractive index, *n* and energy bandgap, Eg that have been proposed by Tripathy,*nT* [70], Moss, n_M [71], Ravindra, n_R [72], Herve-Vandamme (HV), *nHV* [73,74], Reddy and Anjaneyulu, *nRA* [75], Gupta and Ravindra, *nGR* [76], Kumar and Singh, nKS [49] and the empirical equation for each proposal, respectively, as follows:

$$\left.\begin{aligned} n_T &= 1.73 + \left[\left(3.28 \times \exp - (0.539 E_g)\right)\right] \\ n_M &= 3.12199 \times E^{-0.5} \\ n_R &= 4.084 - \left[0.62 \times E_g\right] \\ n_{HV} &= \sqrt{\left(1 + \frac{184.96}{(E_g + 3.47)^2}\right)} \\ n_{RA} &= 3.59182 - \ln(E_g) \\ n_{GR} &= 4.16 - 1.12E_g + 0.3E_g^2 - 0.08E_g^3 \\ n_{KS} &= 3.3668 \times E_g^{-0.32234} \end{aligned}\right\} \quad (27)$$

Values of the refractive indices determined from these methods as a result of the indirect energy bandgap. The dependency of the refractive index on the indirect energy gap are calculated and listed in **Table 10**. The values of the refractive indices behave opposite to that shown by the optical gap energy, as they increase in contrast to the decrease in the optical gap energy Finally, the theoretical values of the refractive index calculated in terms of the gap energy are consistent with the experimental values at the same wavelengths that correspond to the optical gap energy to a large extent, with a slight difference in each approximation and the method of calculation based on it.

IV. CONCLUSION

This study systematically demonstrates that thickness has a decisive impact on the structural, morphological, optical, and electronic properties of $Ge_{20}Cd_{10}Se_{70}$ thin films. Increasing thickness promotes an amorphous-to-crystalline transition, grain growth, and improved crystallinity, while simultaneously reducing strain and defect density. Optical analysis revealed thickness-dependent tuning of refractive index, absorption edge, optical band gap, and Urbach energy, consistent with Mott-Davis and Wemple–DiDomenico models. Furthermore, electronic parameters including dielectric constants, plasma frequency, susceptibility, nonlinear refractive index, and molar refractivity were all strongly influenced by thickness. These results highlight that controlled thickness tailoring can optimize $Ge_{20}Cd_{10}Se_{70}$ thin films for optoelectronic devices.

International Current Journal of Engineering and Science (ICJES)
Volume 4, Issue 11, pp 55-86, November-2025
ISSN (Online): 2583-7257
Article DOI: https://doi.org/10.47001/ICJES/2025.411010

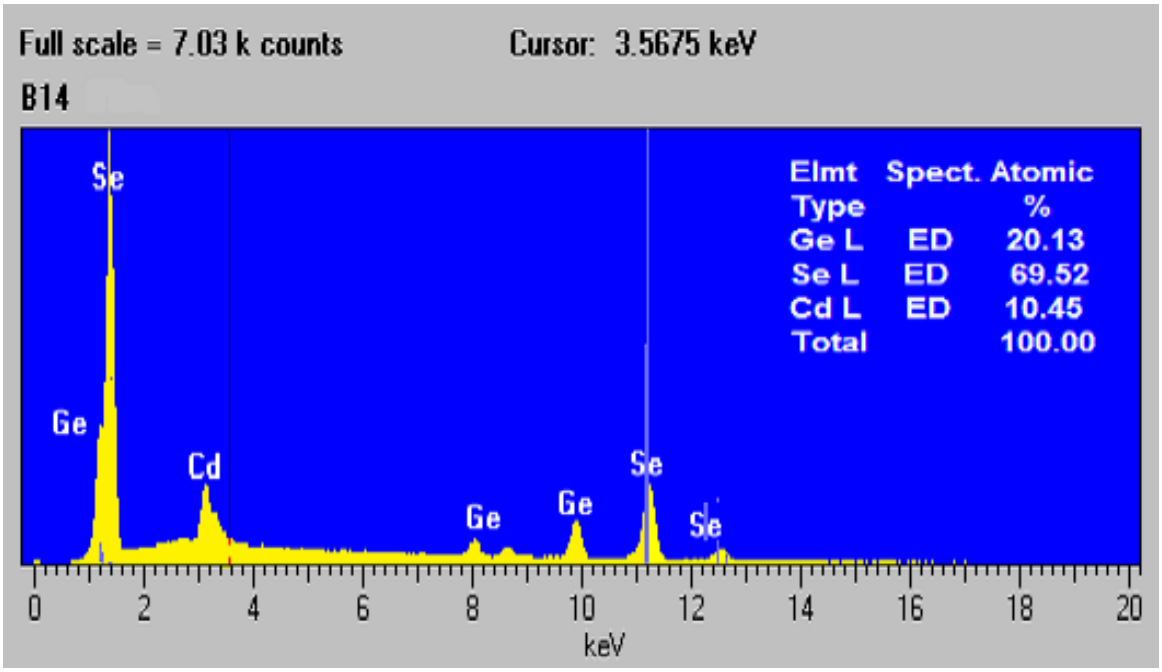

Figure 1: Energy dispersive X-ray (EDX) spectrum of the $Ge_{20}Cd_{10}Se_{70}$ thin films.

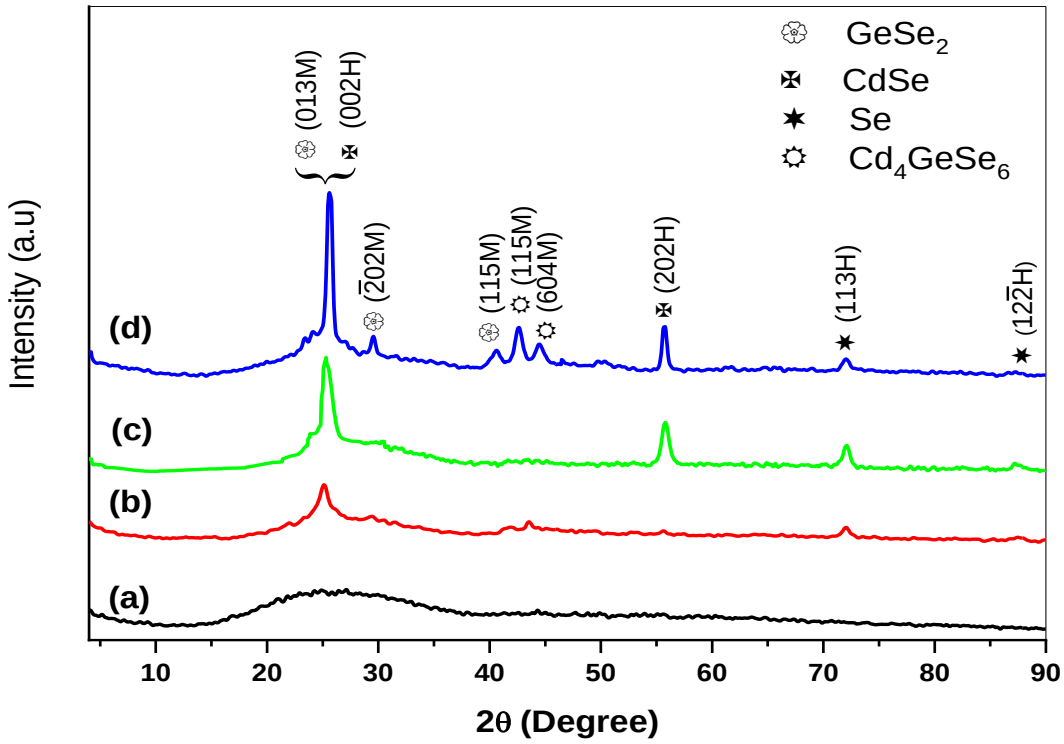

Figure 2: XRD Profiles of $Ge_{20}Cd_{10}Se_{70}$ thin films at different thickness: (a) 200 nm (b) 400 nm (c) 800 nm and (d) 1000 nm

International Current Journal of Engineering and Science (ICJES)
Volume 4, Issue 11, pp 55-86, November-2025
ISSN (Online): 2583-7257
Article DOI: https://doi.org/10.47001/ICJES/2025.411010

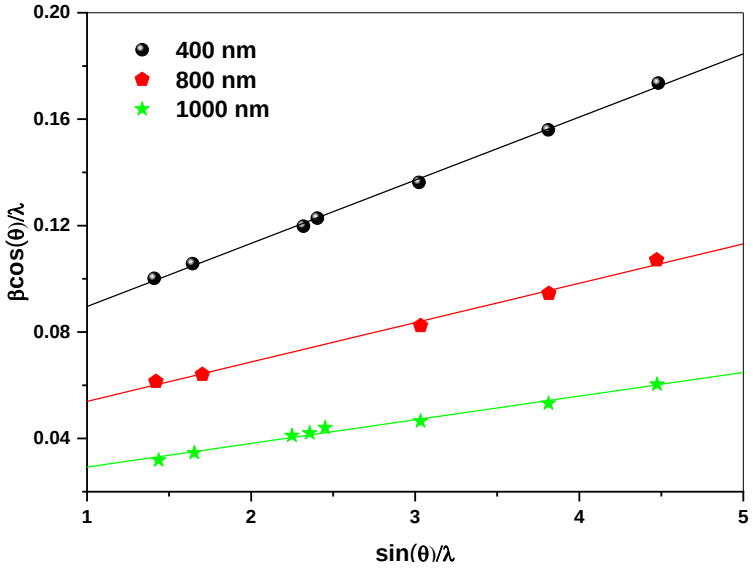

Figure 3: Williamson-Hall plots of $Ge_{20}Cd_{10}Se_{70}$ thin films at different thickness.

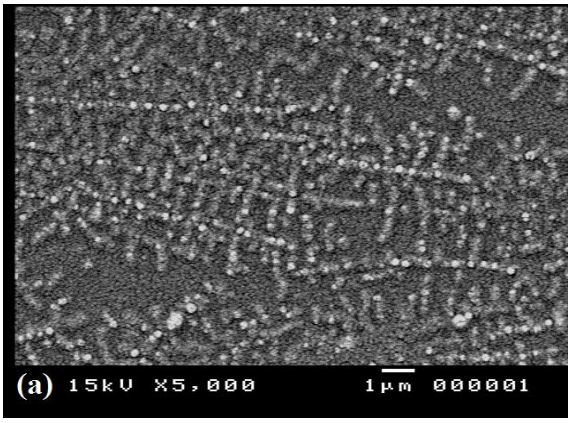

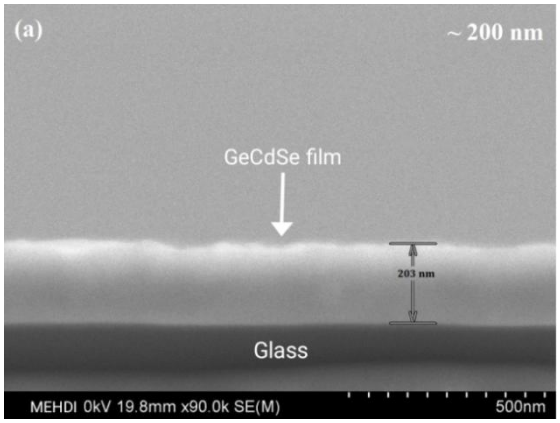

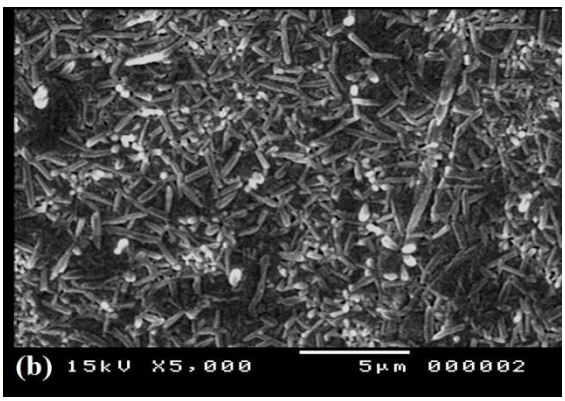

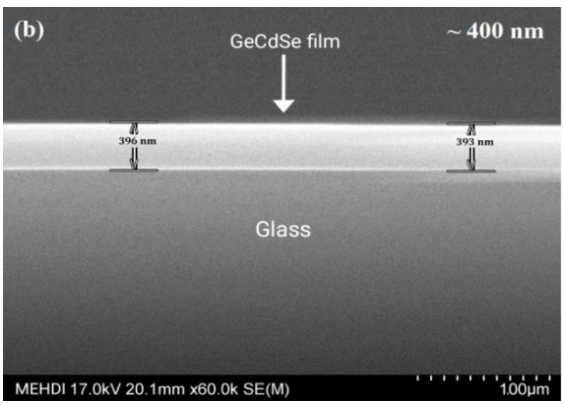

International Current Journal of Engineering and Science (ICJES)
Volume 4, Issue 11, pp 55-86, November-2025
ISSN (Online): 2583-7257
Article DOI: https://doi.org/10.47001/ICJES/2025.411010

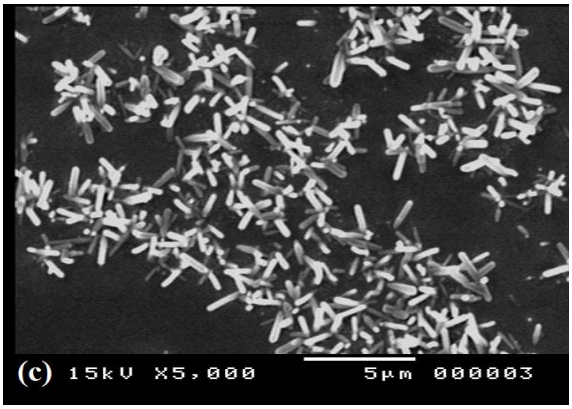

Figure 4: Top view of SEM analysis for $Ge_{20}Cd_{10}Se_{70}$ thin films at different thickness:(a) 200 nm (b) 400 nm (c) 800 nm, and (d) 1000 nm.

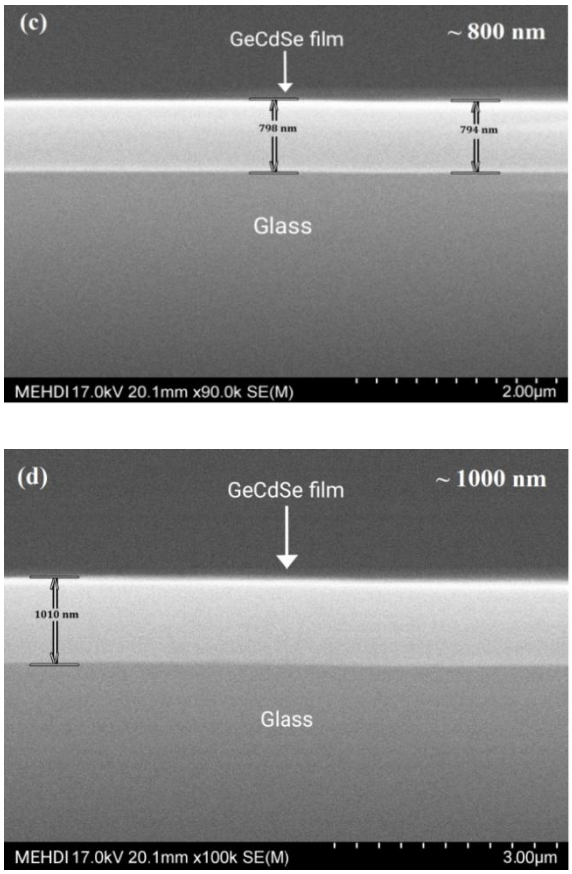

Figure 5: Cross-sections view of SEM analysis for $Ge_{20}Cd_{10}Se_{70}$ thin films at different thickness: (a) 200 nm (b) 400 nm (c) 800 nm, and (d) 1000 nm.

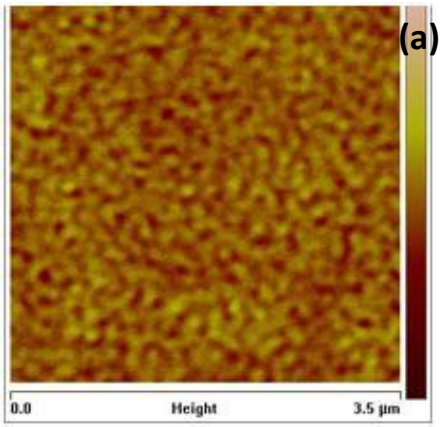

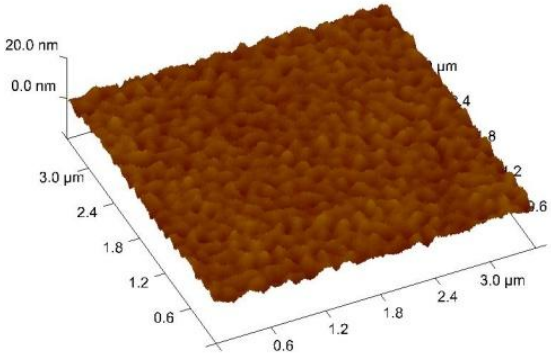

International Current Journal of Engineering and Science (ICJES)
Volume 4, Issue 11, pp 55-86, November-2025
ISSN (Online): 2583-7257
Article DOI: https://doi.org/10.47001/ICJES/2025.411010

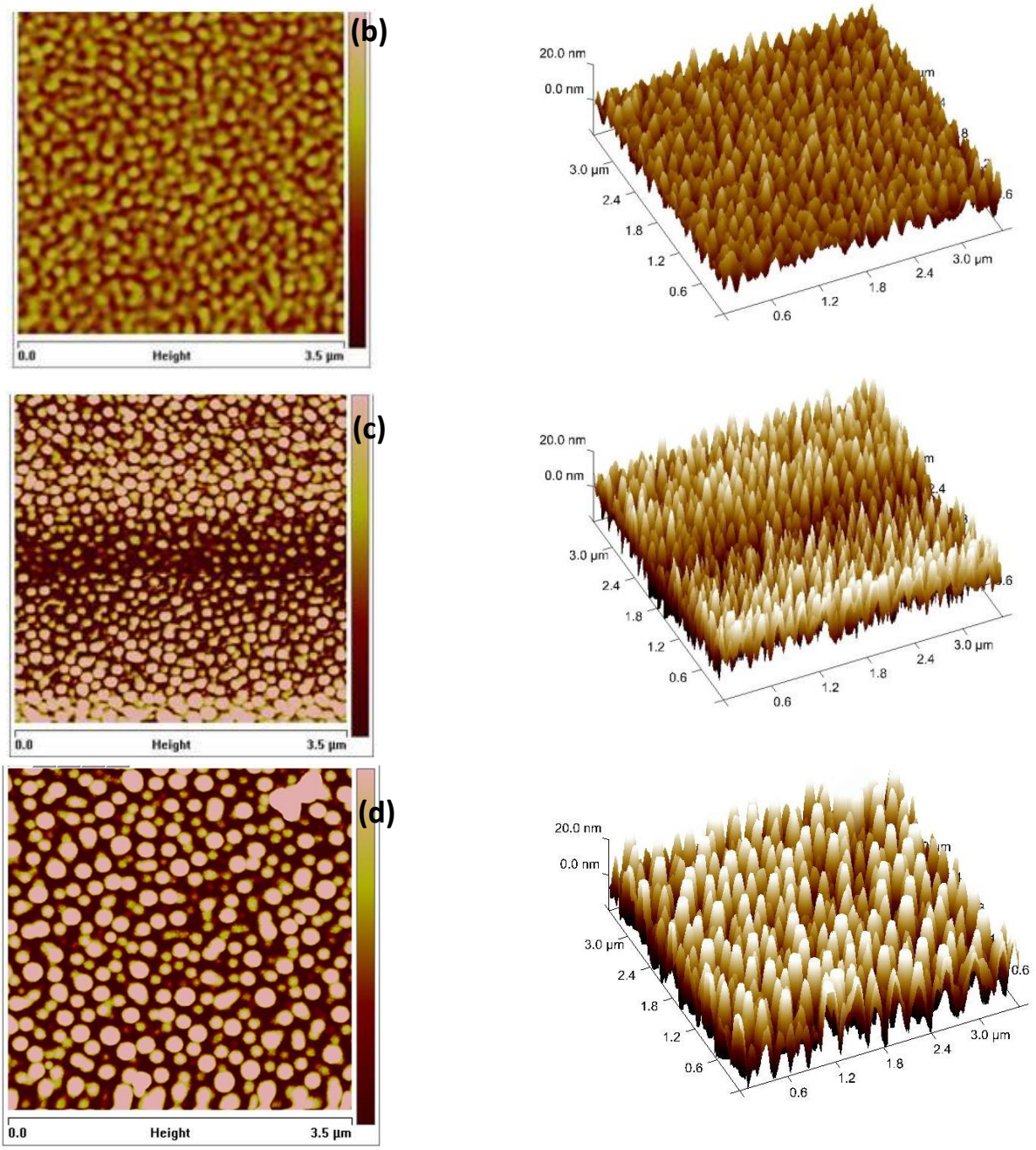

Figure 6: AFM images in 2D and 3D with 3.5×3.5 µm^2 area of $Ge_{20}Cd_{10}Se_{70}$ thin films at different thickness: (a) 200 nm, (b) 400 nm, (c) 800 nm, and (d) 1000 nm.

International Current Journal of Engineering and Science (ICJES)
Volume 4, Issue 11, pp 55-86, November-2025
ISSN (Online): 2583-7257
Article DOI: https://doi.org/10.47001/ICJES/2025.411010

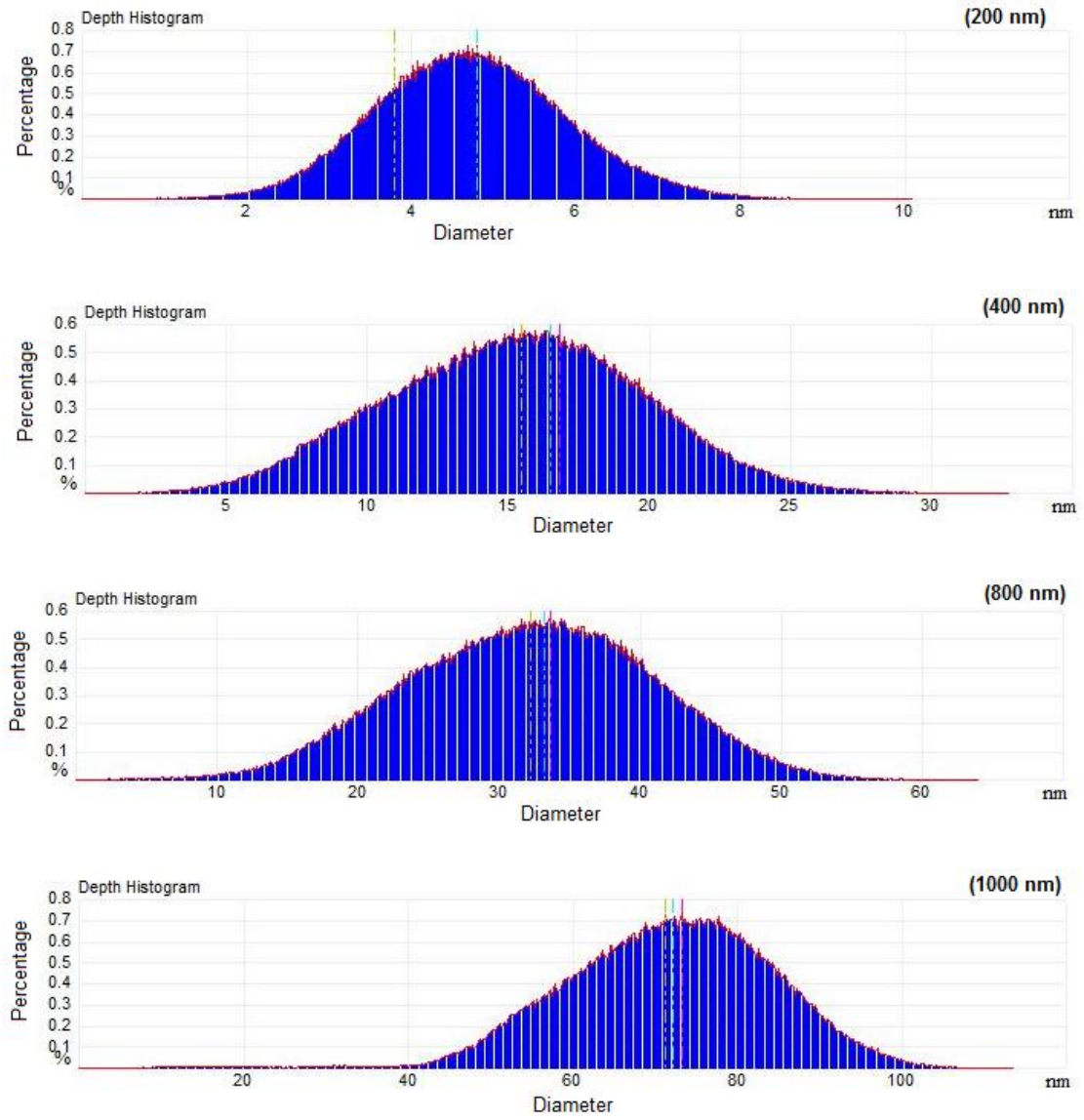

Figure 7: Distribution histogram of the percentage for different thickness of $Ge_{20}Cd_{10}Se_{70}$ thin films as a function of grain diameter

International Current Journal of Engineering and Science (ICJES)
Volume 4, Issue 11, pp 55-86, November-2025
ISSN (Online): 2583-7257
Article DOI: https://doi.org/10.47001/ICJES/2025.411010

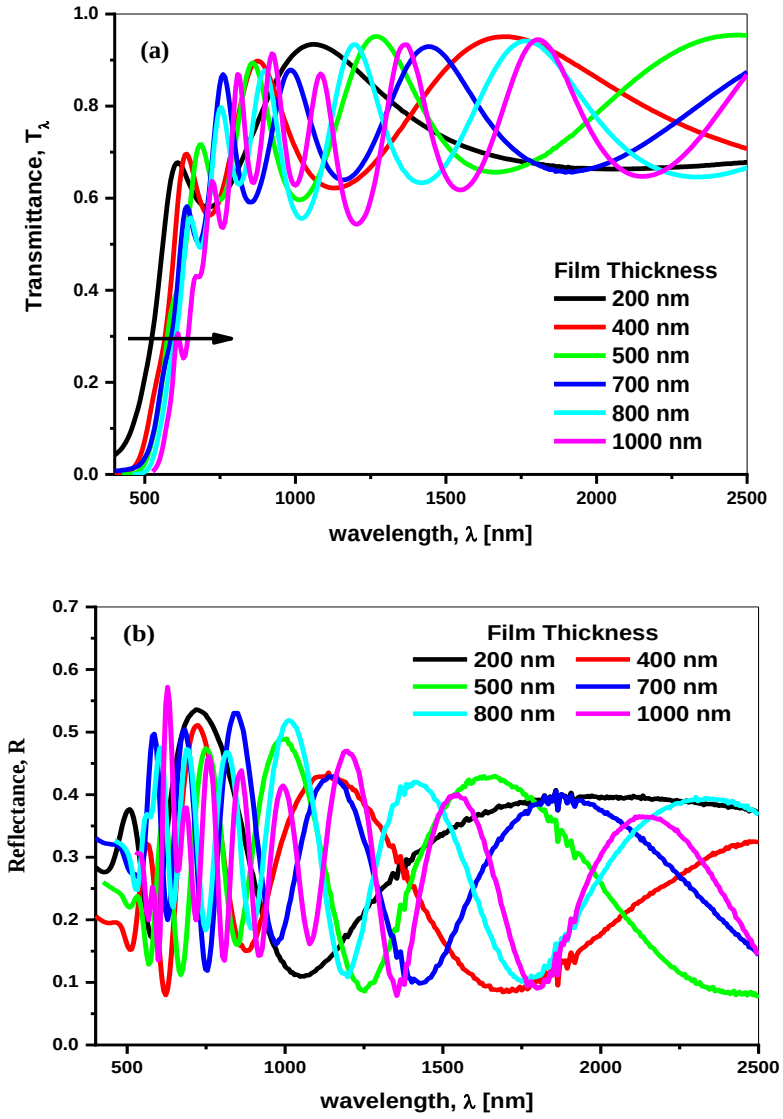

Figure 8: (a) Transmittance and (b) reflectance spectra of Ge20Cd10Se70 thin films at different thickness.

International Current Journal of Engineering and Science (ICJES)
Volume 4, Issue 11, pp 55-86, November-2025
ISSN (Online): 2583-7257
Article DOI: https://doi.org/10.47001/ICJES/2025.411010

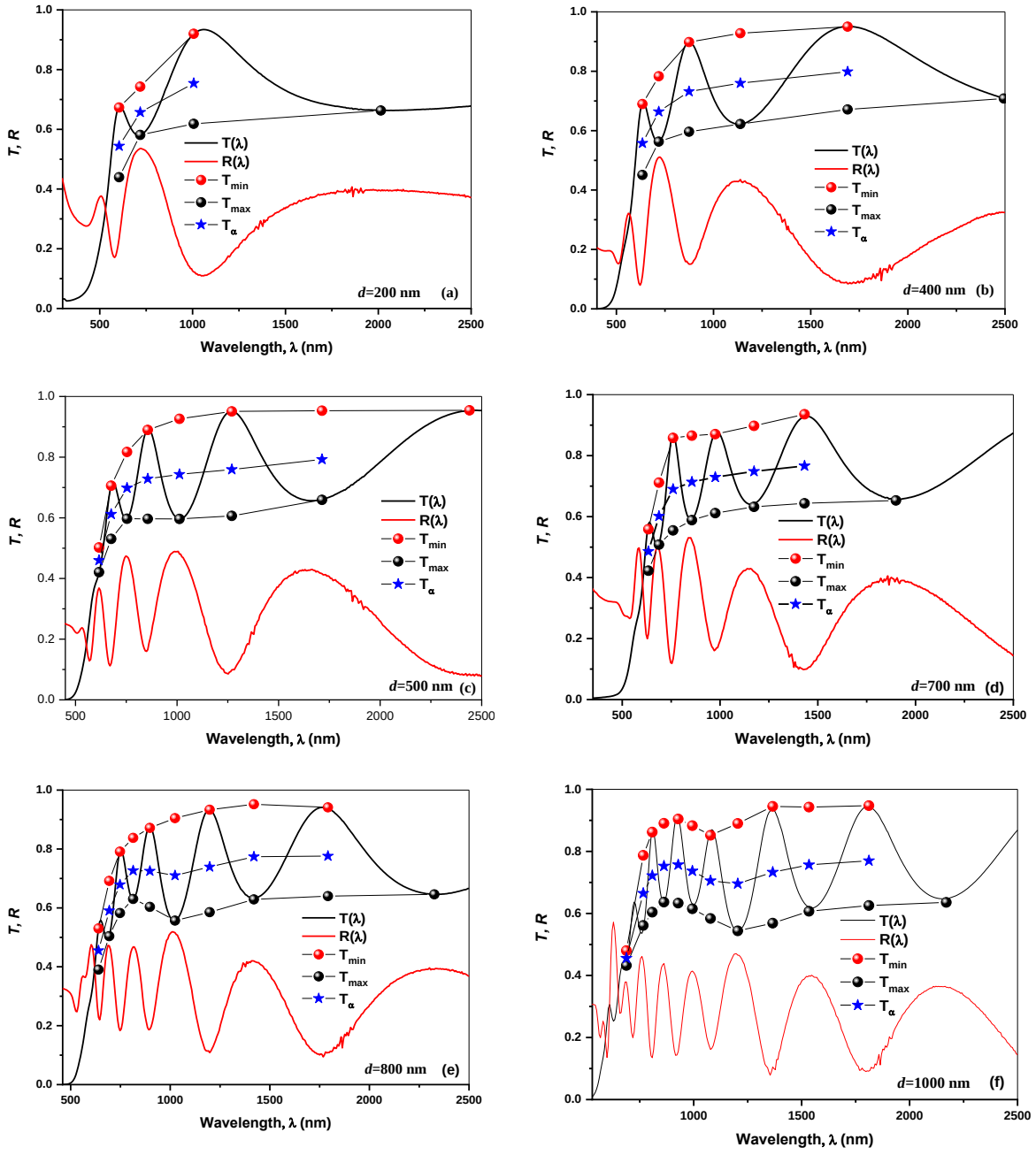

Figure 9: Variation of envelope construction of the typical spectral transmittance and reflectance vs. wavelength of $Ge_{20}Cd_{10}Se_{70}$ thin films at different thickness.

International Current Journal of Engineering and Science (ICJES)
Volume 4, Issue 11, pp 55-86, November-2025
ISSN (Online): 2583-7257
Article DOI: https://doi.org/10.47001/ICJES/2025.411010

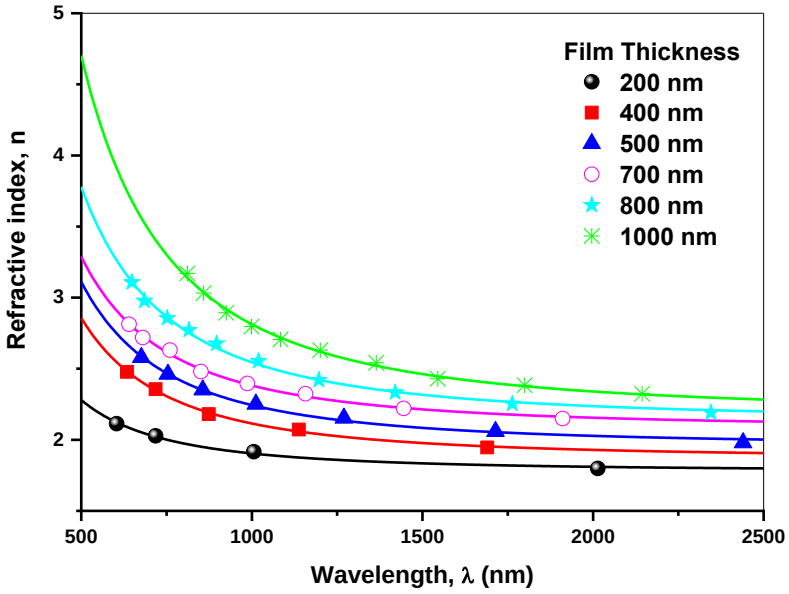

Figure 10: The spectral distribution of the refractive index, n, of $Ge_{20}Cd_{10}Se_{70}$ films at different thickness (the solid lines is the Cauchy's fitting)

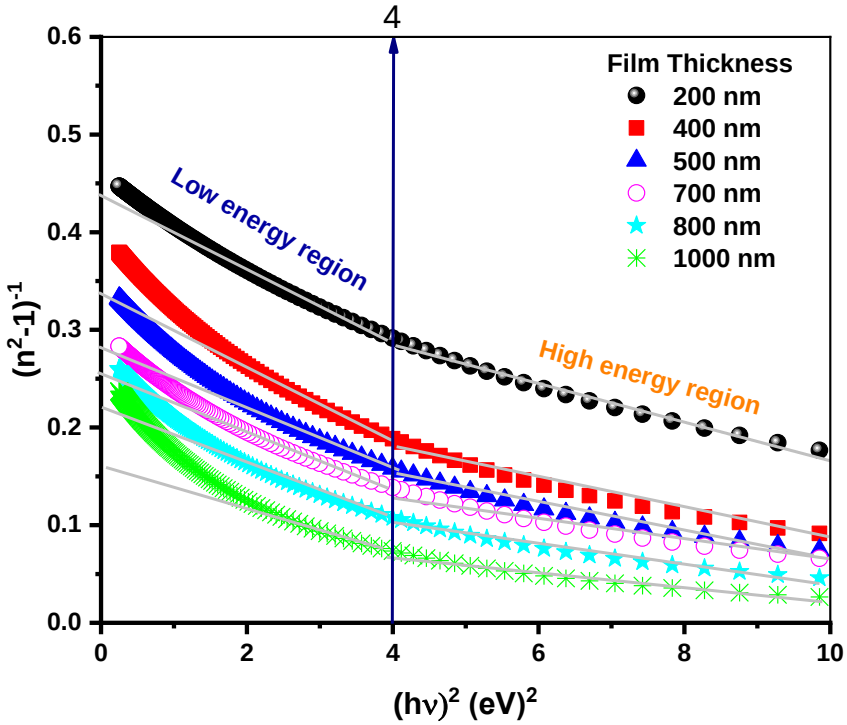

Figure 11: The plot of $(n^2-1)^{-1}$ versus $(h\upsilon)^2$ in the low and high energy regions of $Ge_{20}Cd_{10}Se_{70}$ films at different thickness.

International Current Journal of Engineering and Science (ICJES)
Volume 4, Issue 11, pp 55-86, November-2025
ISSN (Online): 2583-7257
Article DOI: https://doi.org/10.47001/ICJES/2025.411010

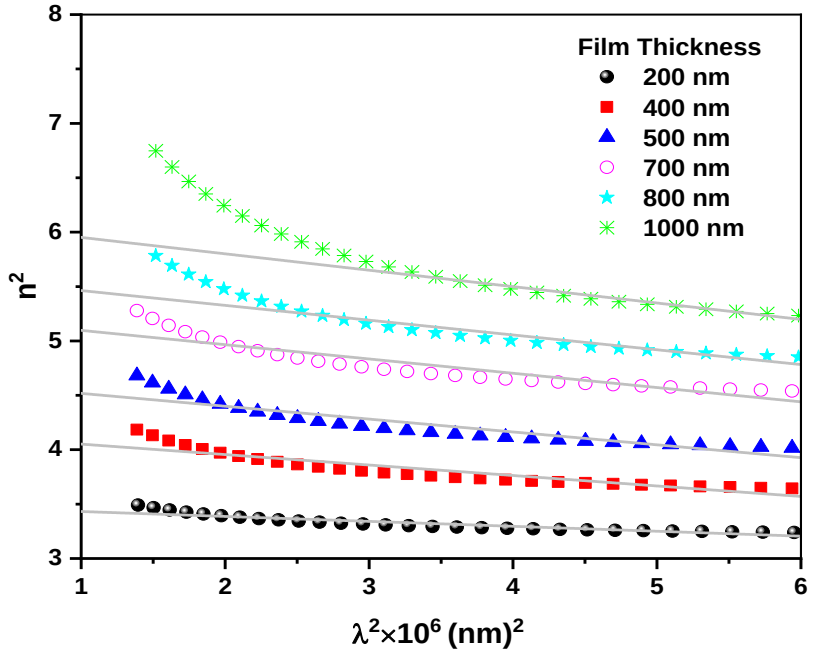

Figure 12: The plot of the relation between n^2 and λ^2 of $Ge_{20}Cd_{10}Se_{70}$ films at different thickness

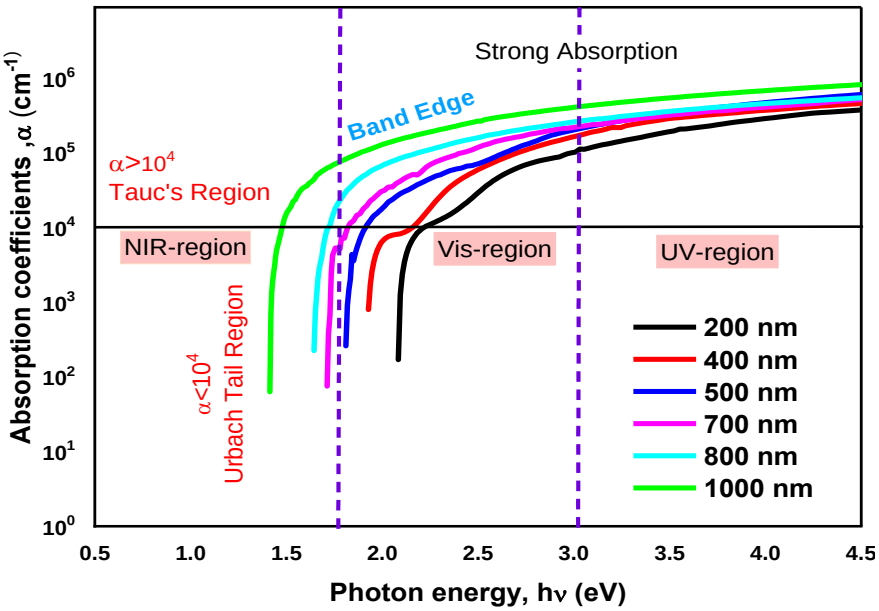

Figure 13: The dependence of the absorption coefficient, α_{opt} on the incident photon energy (hν) of $Ge_{20}Cd_{10}Se_{70}$ thin films at different thickness.

International Current Journal of Engineering and Science (ICJES)
Volume 4, Issue 11, pp 55-86, November-2025
ISSN (Online): 2583-7257
Article DOI: https://doi.org/10.47001/ICJES/2025.411010

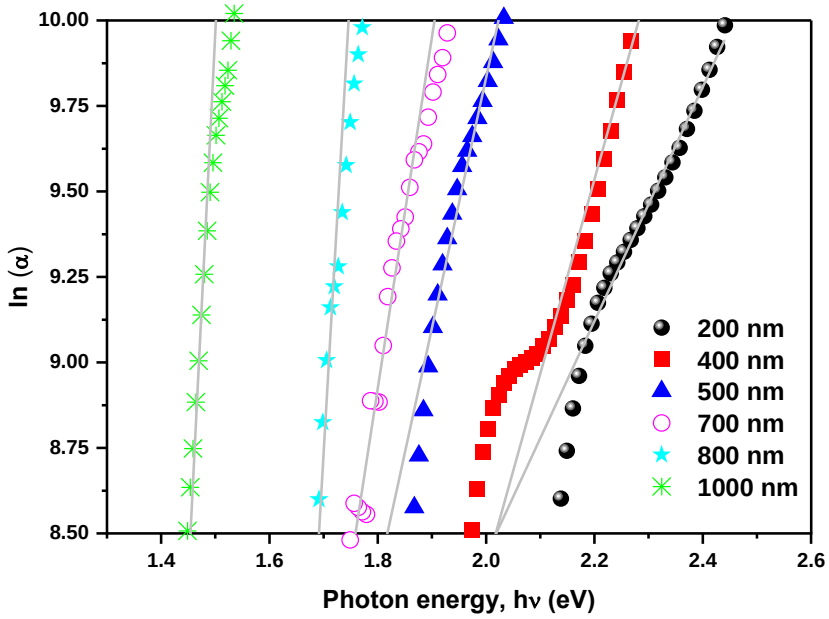

Figure 14: The plot of $\ln(\alpha_{opt})$ versus photon energy, (hν) of $Ge_{20}Cd_{10}Se_{70}$ thin films at different thickness.

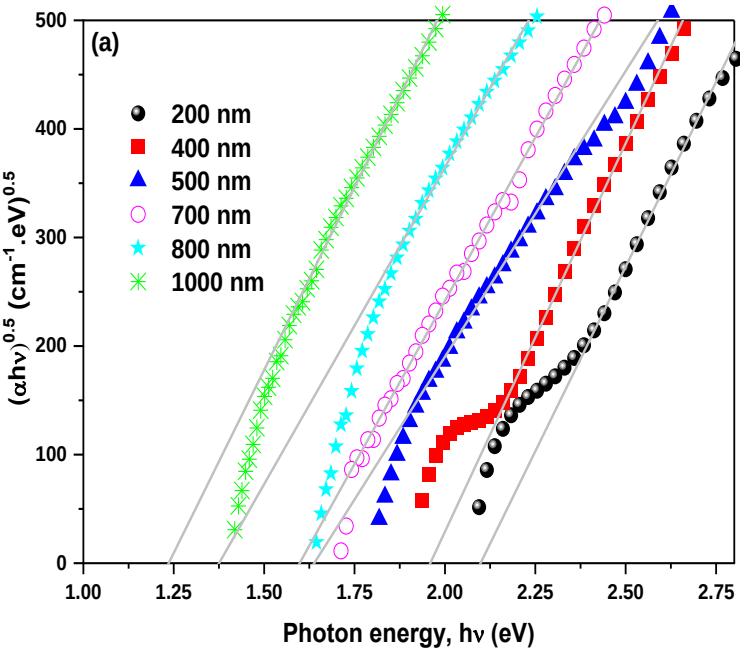

International Current Journal of Engineering and Science (ICJES)
Volume 4, Issue 11, pp 55-86, November-2025
ISSN (Online): 2583-7257
Article DOI: https://doi.org/10.47001/ICJES/2025.411010

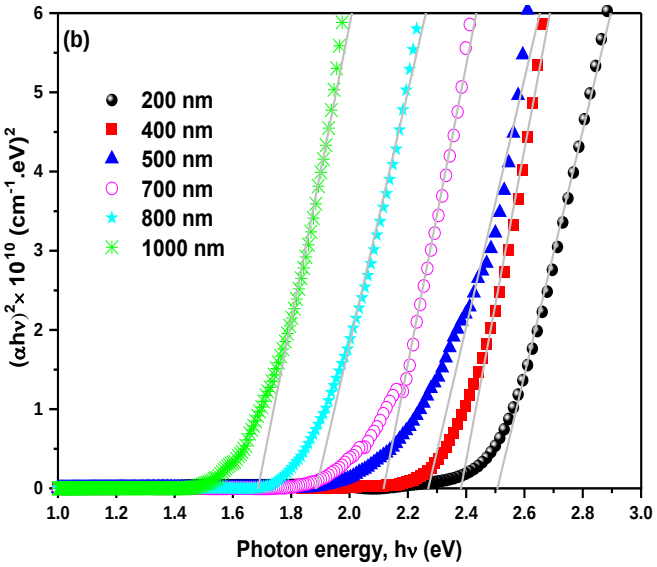

Figure 15: The plot of (a) $(\alpha_{opt}h\nu)^{0.5}$ and (b) $(\alpha_{opt}h\nu)^{2}$ versus photon energy, (hν) of $Ge_{20}Cd_{10}Se_{70}$ thin films at different thickness.

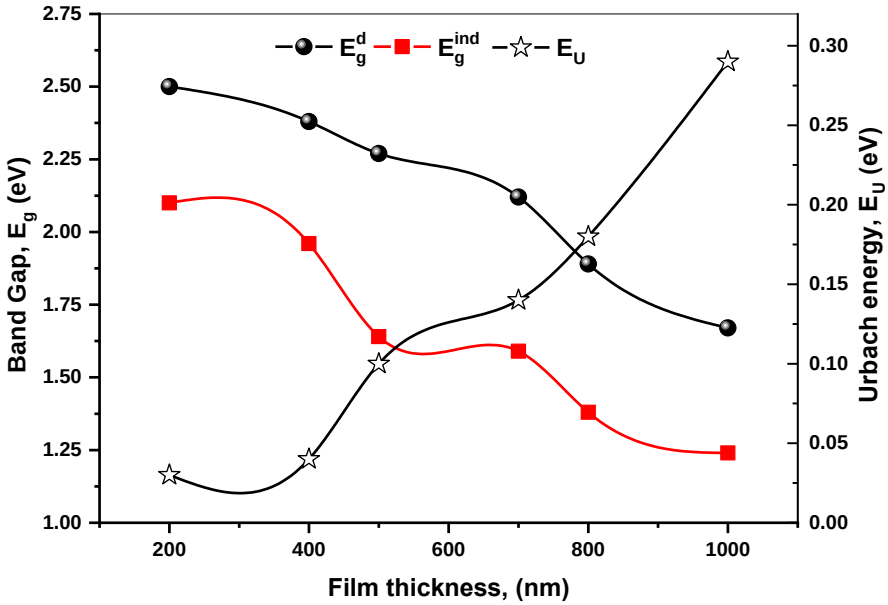

Figure 16: Values of E_g^{opt} and E_U as a function of a film thickness of $Ge_{20}Cd_{10}Se_{70}$ thin films at different thickness.

International Current Journal of Engineering and Science (ICJES)
Volume 4, Issue 11, pp 55-86, November-2025
ISSN (Online): 2583-7257
Article DOI: https://doi.org/10.47001/ICJES/2025.411010

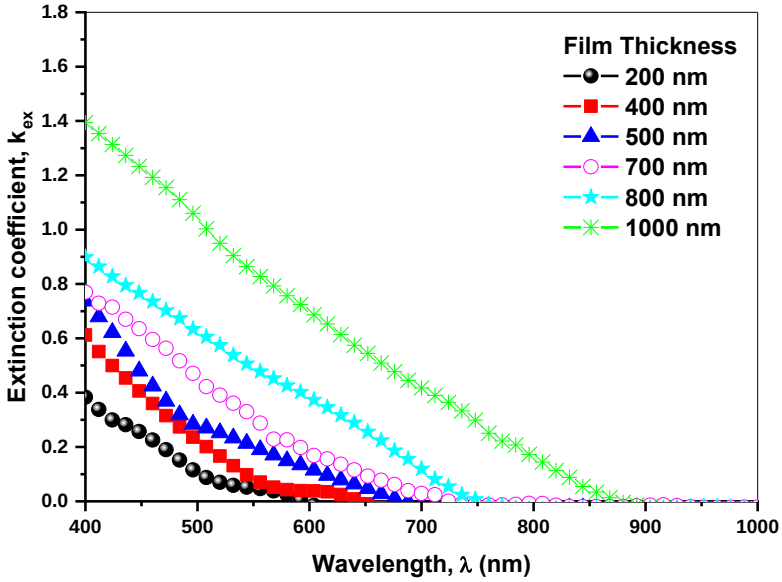

Figure 17: Variation of extinction coefficient, (k_{ex}) vs. wavelength, (λ) of $Ge_{20}Cd_{10}Se_{70}$ thin films at different thickness.

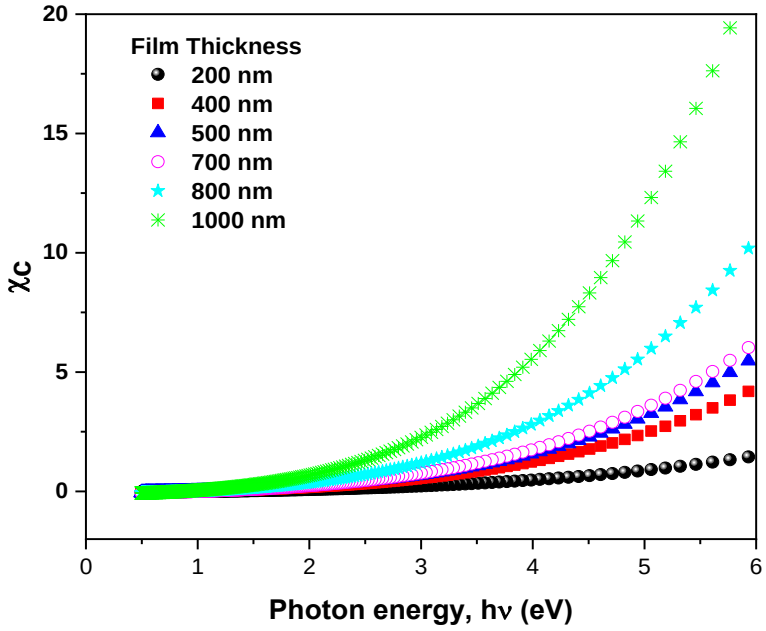

Figure 18: Dependence of the electrical susceptibility, χ_c on photon energy $(h\nu)$ of $Ge_{20}Cd_{10}Se_{70}$ thin films at different thickness.

International Current Journal of Engineering and Science (ICJES)
Volume 4, Issue 11, pp 55-86, November-2025
ISSN (Online): 2583-7257
Article DOI: https://doi.org/10.47001/ICJES/2025.411010

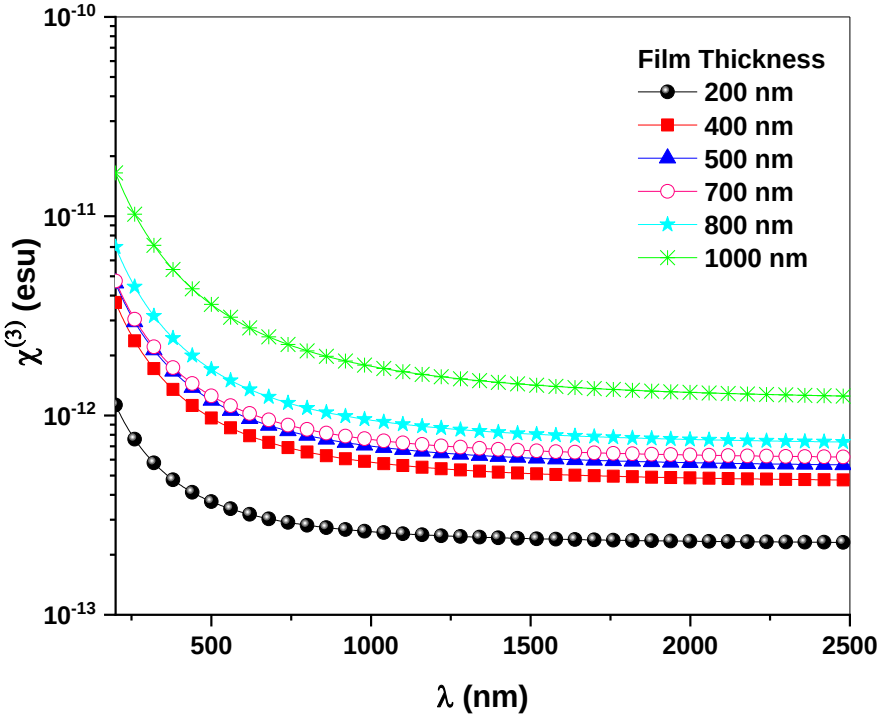

Figure 19: Dependence of non-linear the third order optical, $\chi^{(3)}$ on the wavelength for the investigated films.

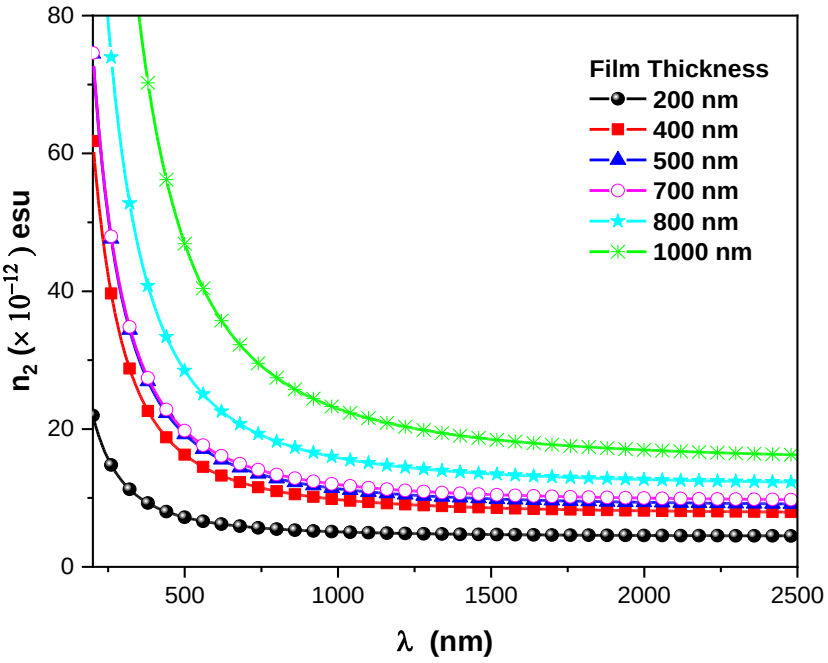

Figure 20: Dependence of non-linear second-order refractive index, n_2 on the wavelength for of $Ge_{20}Cd_{10}Se_{70}$ thin films at different thickness according to Boling relationship

International Current Journal of Engineering and Science (ICJES)
Volume 4, Issue 11, pp 55-86, November-2025
ISSN (Online): 2583-7257
Article DOI: https://doi.org/10.47001/ICJES/2025.411010

Table 1: Stractural parameters of $Ge_{20}Cd_{10}Se_{70}$ thin films at different thickness.

Film Thickness (nm)	2θ (Degree) Obs.	2θ (Degree) Stand.	h k ℓ plane	Phase	JCPDS file No.
200	--	--	---	Amorphous	---
400	25.12	25.371	123(M)	GeSe2	71-0117
		25.281	002(H)	CdSe	02-0330
	29.38	29.433	$\bar{2}02$(M)	GeSe2	71-0117
	41.92	41.829	330(M)	GeSe2	71-0117
	43.54	43.613	135(M)	GeSe2	71-0117
	55.6	55.695	202(H)	CdSe	02-0330
	72.54	72.745	113(H)	Se	86-2244
	87.46	87.562	$12\bar{2}$(H)	Se	85-0569
800	25.3	25.371	123(M)	GeSe2	71-0117
		25.281	002(H)	CdSe	02-0330
	30.46	30.394	$\bar{1}33$(M)	GeSe2	71-0117
	55.78	55.695	202(H)	CdSe	02-0330
	72.43	72.745	113(H)	Se	86-2244
	87.22	87.562	$12\bar{2}$(H)	Se	85-0569
1000	25.6	25.371	123(M)	GeSe2	71-0117
		25.281	002(H)	CdSe	02-0330
	29.56	29.433	$\bar{2}02$(M)	GeSe2	71-0117
	40.6	40.713	115(M)	GeSe2	71-0117
	42.64	42.646	115(M)	Cd4GeSe6	22-0122
	44.44	44.996	604(M)	Cd4GeSe6	22-0122
	55.78	55.695	202(H)	CdSe	02-0330
	72.44	72.745	113(H)	Se	86-2244
	87.28	87.562	$12\bar{2}$(H)	Se	85-0569

Table 2: Structural parameters viz. average crystalline Size, micro-strain, dislocation density, and crystallites per unit surface area values of polycrystalline $Ge_{20}Cd_{10}Se_{70}$ thin films at different thickness.

Film thickness (nm)	Average of crystallite size (nm)	Micro-strain (ε) × 10^{-3} ($lin^{-2}.m^{-4}$)	Dislocation density δ× 10^{14} ($lines/m^2$)	Crystallites per unit surface area N× 10^{16} ($Crys/m^2$)
400	14.27	5.93	49.10	13.76
800	24.00	3.70	17.35	5.78

International Current Journal of Engineering and Science (ICJES)
Volume 4, Issue 11, pp 55-86, November-2025
ISSN (Online): 2583-7257
Article DOI: https://doi.org/10.47001/ICJES/2025.411010

1000	41.87	2.22	5.70	0.14

Table 3: RMS Surface roughness, Average surface roughness, and Average grain size values of $Ge_{20}Cd_{10}Se_{70}$ thin films

Film thickness (nm)	RMS Surface roughness, Rq(nm)	Average surface roughness, Ra(nm)	Average grain size (nm)
200	1.15	0.91	4.81
400	4.43	3.58	16.5
800	8.57	6.95	32.2
1000	12.70	10.00	72.1

Table 4: Values of the Cauchy coefficient parameters (a, b) and film thickness.

Film Thickness (nm)	Cauchy coefficient $n = a + b/\lambda^2$		Calculated film Thickness (nm)
	a	b $\times 10^5$ $(nm)^2$	
200	1.77878	1.25166	207.77
400	1.86718	2.47444	398.38
500	1.95556	2.88775	502.72
700	2.07986	3.02048	707.52
800	2.13375	4.11521	796.33
1000	2.18236	6.30131	1018.82

Table 5: dispassion parameters and high dielectric constants in low and high energy regions of $Ge_{20}Cd_{10}Se_{70}$ films at different thickness

Film Thickness (nm)	Low energy region				High energy region			
	$\hat{E}_o$ (eV)	$\hat{E}_d$ (eV)	$\hat{n}_0$	$\hat{\varepsilon}_\infty$	E_o eV	E_d (eV)	n_0	ε_∞
200	3.19	7.02	1.79	3.20	4.29	11.78	1.94	3.75
400	2.61	6.77	1.90	3.60	3.85	15.63	2.25	5.06
500	2.55	7.54	1.99	3.96	3.57	15.87	2.33	5.44
700	2.59	8.99	2.12	4.47	3.38	15.97	2.39	5.72
800	2.39	9.06	2.19	4.79	3.13	17.24	2.55	6.50
1000	2.16	9.11	2.28	5.22	2.96	21.92	2.90	8.41

Table 6: The values of the lattice dielectric constants, the plasma resonance frequency, the oscillator wavelength, and the oscillator strength, of $Ge_{20}Cd_{10}Se_{70}$ films at different thickness.

Film thickness (nm)	ε_L	N/m^* $\times 10^{55}$ $[m^{-3}.kg^{-1}]$	ω_p $\times 10^{14}$ Hz	The oscillator wavelength, λ_o (nm)	The oscillator strength, S_o $\times 10^{13}$ (m^{-2})	The ratio of E_o/S_o $\times 10^{-14}$ $(eV.m^2)$

International Current Journal of Engineering and Science (ICJES)
Volume 4, Issue 11, pp 55-86, November-2025
ISSN (Online): 2583-7257
Article DOI: https://doi.org/10.47001/ICJES/2025.411010

200	3.48	1.77	1.21	289.19	3.29	9.7
400	4.15	3.76	1.62	321.98	3.92	6.7
500	4.64	4.62	1.70	347.21	3.69	6.9
700	5.23	5.14	1.69	366.27	3.52	7.4
800	5.60	5.32	1.66	395.62	3.51	6.8
1000	6.10	5.89	1.67	418.96	4.22	5.1

Table 7: The values of band gap and Urbach Energies of $Ge_{20}Cd_{10}Se_{70}$ films at different thickness.

Film thickness (nm)	Direct Band Gap $E_g^d(eV)$	Indirect Band Gap $E_g^{ind}(eV)$	Urbach Energy E_U (eV)
200	2.5	2.1	0.03
400	2.38	1.96	0.04
500	2.27	1.64	0.10
700	2.12	1.59	0.14
800	1.89	1.38	0.18
1000	1.67	1.24	0.29

Table 8: Electronic parameters are including (Plasmon energy ψ , Penn energy E_P , Fermi energy E_F and the number of effective electrons n_{eff} of $Ge_{20}Cd_{10}Se_{70}$ thin films at different thickness.

Film thickness (nm)	$\chi^{(1)}$ esu	$\chi^{(3)}$ ($\times 10^{-10}$ esu)	n2	Ψ (ev)	Ep (ev)	Ef (ev)	neff (electron)
200	0.2188	0.0039	0.0758	0.0799	0.0507	0.0101	0.01181
400	0.3232	0.0185	0.3107	0.1066	0.0600	0.0149	0.02102
500	0.3538	0.0266	0.4303	0.1117	0.0586	0.0158	0.02308
700	0.3756	0.0338	0.5334	0.1109	0.0539	0.0157	0.02275
800	0.4379	0.0625	0.9245	0.1091	0.0508	0.0153	0.02201
1000	0.5897	0.2056	2.6718	0.1100	0.0487	0.0155	0.02238

Table 9: The electronic polarization α_P according several empirical formulas mentioned in text and molar refractivity R_m of $Ge_{20}Cd_{10}Se_{70}$ thin films at different thickness.

Film thickness (nm)	Eq.(21)	Eq.(22)	Eq.(5.23)	Eq.(5.24)	Eq.(5.25)	Based on	Based on

International Current Journal of Engineering and Science (ICJES)
Volume 4, Issue 11, pp 55-86, November-2025
ISSN (Online): 2583-7257
Article DOI: https://doi.org/10.47001/ICJES/2025.411010

200	2.74584	4.53416	4.33119	3.90441	1.65593	6.587	7.443
400	3.10863	4.58944	4.39991	3.97789	2.06452	7.221	8.952
500	3.32616	4.72924	4.56159	4.15641	2.14327	7.736	9.294
700	3.55138	4.7531	4.58753	4.18583	2.19225	8.355	9.517
800	3.67444	4.86638	4.70436	4.32114	2.30766	8.694	10.074
1000	3.82324	4.94098	4.77582	4.40626	2.49301	9.097	11.080

Table 10: The refractive index-energy band-gap dependence of $Ge_{20}Cd_{10}Se_{70}$ thin films at different thickness.

Film thickness (nm)	n_T	n_M	n_R	n_{HV}	n_{RA}	n_{GR}	n_{KS}	$\bar{n}$
200	2.7907	2.5934	2.782	2.63849	2.8498	2.434	2.650	2.677
400	2.8738	2.6385	2.8688	2.69685	2.9188	2.553	2.7102	2.751
500	3.0892	2.7588	3.0672	2.84311	3.0971	2.804	2.8705	2.932
700	3.1263	2.7802	3.0982	2.86774	3.1280	2.841	2.8993	2.963
800	3.3021	2.8857	3.2346	2.98255	3.2770	3.002	3.0419	3.103
1000	3.4162	2.9585	3.3152	3.05573	3.376	3.095	3.1412	3.194

REFERENCES

[1] A.B. Seddon, Z. Q. Tang, D. Furniss, S. Sujecki, T. M. Benson, "Progress in rare-earth-doped mid-infrared fiber lasers." Optics express 18.25 (2010): 26704-26719.

[2] J. Heo, W. J. Chung, " in Chalcogenide Glasses: Preparation, Properties and Applications, Edited by J.-L. Adam and X. Zhang. Woodhead Publishing, Oxford, (2014), 347–80.

[3] A.B. Seddon, M. J. Laine, "Chalcogenide glasses for acousto-optic devices. II. As–Ge–Se systems", Non Cryst. Solids, 213 (1997) 168-173.

[4] A.Ganjoo, H. Jain, C. Yu, R. Song, J. V. Ryan, J. Irudayaraj, Y. J Ding, C. G. Pantano, "Planar chalcogenide glass waveguides for IR evanescent wave sensors.", Non Cryst. Solids, 352.6-7 (2006) 584-588.

[5] D. R. Simons, A. J. Faber, H. Waal, "GeSx glass for Pr3+-doped fiber amplifiers at 1.3 μm.", Non Cryst. Solids 185.3 (1995): 283-288

[6] G-F Zhou, "Materials aspects in phase change optical recording.", Mater. Sci. Eng. : A 304 (2001) 73-80

[7] R. Swanepoel, "Determination of surface roughness and optical constants of inhomogeneous amorphous silicon films." J. Phys. E: Sci. Instrum. 17.10 (1984): 896-903.

[8] A.Dahshan, K.A. Aly, "Optical constants of new amorphous As–Ge–Se–Sb thin films." Acta Mater. 56.17 (2008) 4869-4875

[9] K.A. Aly, A. Dahshan, A.M. Abousehly, "Compositional dependence of the optical properties of amorphous Se_{100-x} Te_x thin films.", Philos. Mag. 88.1 (2008) 47-60.

[10] Y. Wada, Y. Wang, O. Matsuda, K. Inoue, K. Murase, "Photoluminescence study of glassy Ge $(S_xSe_{1-x})_2$.", J. Non-Cryst. Solids, 198 (1996) 732-735.

[11] A. Feltz, H. Aust, A. Blayer, "Glass formation and properties of chalcogenide systems XXVI: Permittivity and the structure of glasses As_xSe_{1-x} and $GexSe_{1-x}$." J. Non-Cryst. Solids, 55.2 (1983): 179-190

International Current Journal of Engineering and Science (ICJES)
Volume 4, Issue 11, pp 55-86, November-2025
ISSN (Online): 2583-7257
Article DOI: https://doi.org/10.47001/ICJES/2025.411010

[12] S. Asokan, G. Parthasarathy, E.S.R. Gopal, "High-pressure studies on Ge-Te glasses. Evidence for a critical composition in IV-VI chalcogenide glassy systems.", Philos. Mag. B 57.1 (1988): 49-60.
[13] Z.G. Ivanova, V.S. Vassilev, S.V. Boycheva, N. Kirov, "Topological transition and rigidity percolation in Ge–Se (S)–Cd glasses." J. Non-Cryst. Solids, 232 (1998): 274-277.
[14] A.B. Alwany, B. Hassan, Y. Alajlani, A. Alnakhlani, R.. A. Fouad, "Analyzing the Influence of Varying Film Thickness on the Structural and Optical Properties of $Ge_{15}Se_{75}Zn_{10}$ Thin Films. J Inorg Organomet Polym 35, 838–845 (2025).
[15] George F. Harrington, José Santiso, "Back-to-Basics tutorial: X-ray diffraction of thin films", Journal of Electroceramics, 47.4 (2021) 141-163.
[16] G. K. Williamson and W. H, Hall, " X-ray line broadening from filed aluminium and wolfram" Acta Metallurgica, 1.1 (1953) 22-31.
[17] G. A. Dorofeev, A. N. Streletskii, I. V. Povstugar, A. V. Protasov, & E. P. Elsukov, Determination of nanoparticle sizes by X-ray diffraction. Colloid Journal, 74(6) (2012) 675-685.
[18] A. Stokes, A. Wilson, "The diffraction of X rays by distorted crystal aggregates-I." Proceedings of the physical society 56.3 (1944) 174-181.
[19] G. K. Williamson and R. E. Smallman, "III. Dislocation densities in some annealed and cold-worked metals from measurements on the X-ray Debye-Scherrer spectrum", Philos. Mag., 1(1), (1956) 34-45.
[20] A. Alqahtani, H. A. Alrafai , M. Al-Dossari, E. R. Shaaban, Ammar Qasem, "A profound analysis of structural, thermal, optical, and electrical properties of $Cd_{50}Pb_{30}S_{20}$ composition for optoelectronic devices: implications of changes in film's thickness" Optical and Quantum Electronics (2023) 55:18-53.
[21] H.I. Efkere, A. Tataroglu, S.S. Cetin, N. Topaloglu, M. Polat Gonullu, H. Ates, "The Effect of Thickness on the Optical, Structural and Electrical Properties of ZnO Thin Film Deposited on n type Si", Journal of Molecular Structure 1165 (2018): 376-380.
[22] N. kumar, U. Parihar, R. Kumar, K. J. Patel, C. J. Panchal, N. Padha, " Effect of Film Thickness on Optical Properties of Tin Selenide Thin Films Prepared by Thermal Evaporation for Photovoltaic Applications" American Journal of Materials Science, 2(1) (2012) 41-45.
[23] Dhaval Vankhade, Tapas K. Chaudhuri, "Effect of thickness on structural and optical properties of spin-coated nanocrystalline PbS thin films" Optical Materials, 98 (2019): 109491.
[24] S. Atta. M. Hiba M. Ali "The Thickness Effects Characterization Properties Of Copper Oxide Thin Films Prepared By Thermal Evaporation Technique", Journal of Multidisciplinary Engineering Science Studies (JMESS), 2 (5)(2016) 532-535.
[25] R. Swanepoel, "Determination of the thickness and optical constants of amorphous silicon." J. Phys. E: Sci. Instrum. 1. 12(1983) 1214-1222.
[26] E.R. Shaaban, M.Y. Hassaan, M.G. Moustafa, Ammar Qasem, Goma A.M. Alid, El Sayed Yousef, "Optical constants, dispersion parameters and non-linearity of different thickness of $As_{40}S_{45}Se_{15}$ thin films for optoelectronic applications", Optik - International Journal for Light and Electron Optics 186 (2019) 275–287.
[27] T. S. Moss, "optical properties of semiconductors" , (Butterworths, London), (1959).
[28] J.C. Manifacier, J. Gasiot, J.P. Fillard, "A simple method for the determination of the optical constants n, k and the thickness of a weakly absorbing thin film." Journal of Physics E: Scientific Instruments 9.11 (1976): 1002.
[29] S. H. Wemple, DiDomenico, Behavior of the Electronic Dielectric Constant in Covalent and Ionic Materials, Phys. Rev. B 3,(1971) 1338
[30] S.H. Wemple, "Refractive-index behavior of amorphous semiconductors and glasses." , Phys. Rev. B 7.8 (1973): 3767.
[31] Ammar Qasem , M.Y. Hassaan , M.G. Moustafa , Mohamed A.S. Hammam , H. Y. Zahran , I.S. Yahia E.R. Shaaban , "Optical and electronic properties for As-60 at.% S uniform thickness of thin films: Influence of Se content" Optical Materials 109 (2020) 110257.

International Current Journal of Engineering and Science (ICJES)
Volume 4, Issue 11, pp 55-86, November-2025
ISSN (Online): 2583-7257
Article DOI: https://doi.org/10.47001/ICJES/2025.411010

[32] M. A. Dabban, Nema M. Abdelazim, Alaa M. Abd-Elnaiem, S. Mustafa and M. A. Abdel-Rahim," Effect of Sn substitution for Se on dispersive optical constants of amorphous Se–Te–Sn thin films", Materials Research Innovations", 22:6 (2018) 324-332.

[33] H. Ticha, L. Tichy, Semiempirical relation between non-linear susceptibility (refractive index), linear refractive index and optical gap and its application to amorphous chalcogenides, J.Optoelectron. Adv. Mater., 4 (2002) 381-386.

[34] T. Tanaka, "Optical properties and photoinduced changes in amorphous As-S films." Thin solid films 66.3 (1980): 271-279.

[35] K. Tanaka, "Structural phase transitions in chalcogenide glasses", Phys. Rev. B 39 (1989) 1270.

[36] A.S. Hassanien, "Studies on dielectric properties, opto-electrical parameters and electronic polarizability of thermally evaporated amorphous Cd50S50− xSex thin films." J. of Alloys and Compounds 671 (2016): 566-578.

[37] H. M. Kotb, M. A. Dabban, A. Y. M. M. Hafiz, "Annealing temperature dependence of the optical and structural properties of selenium-rich CdSe thin films", J. of alloys and compounds, 512(1) (2012)115-120.

[38] M. El-Nahass, E. El-Menyawy, "Thickness dependence of structural and optical properties of indium tin oxide nanofiber thin films prepared by electron beam evaporation onto quartz substrates", Materials Science and Engineering: B, 177 (2012) 145-150.

[39] F. Yakuphanoglu, C. Viswanathan, "Electrical conductivity and single oscillator model properties of amorphous CuSe semiconductor thin film", *J. Non-Cryst. Solids* 353 (2007) 2934-2937.

[40] M. M. Malik, M. Zulfequar, A. Kumar, M. Husain, "Effect of indium impurities on the electrical properties of amorphous Ga30Se70". J. Phys. Condens. Matter, 4(43) (1992) 8331.

[41] M. M. Hafiz, H. Mahfoz Kotb, M. A. Dabban, and A. Y. Abdel-latif, "Optical properties of $Cd_{20}Se_{80-x}M_x$ (M: Zn, In, and Sn) thin film alloys", Optics & Laser Technology 49 (2013) 188–195.

[42] N.A. Subrahamanyam, A Textbook of Optics, 9th ed., Brj Laboratory, Delhi, India 1977.

[43] Abdulnasser Alfaqeer, Ahmed lrebati, Mehdi Dabban, "Extraction of Optical Constants and Dispersion Parameters of CdTe/CdSe Bi-Layer Thin Films" The scientific Journal of university of Saba region, 5:1 (2022) 241-278.

[44] M. Didomenico, S. H. Wemple, "Oxygen-octahedra ferroelectrics. I. Theory of electro-optical and nonlinear optical effects", *J. Appl. Phys.*, 40 (1969) 720-734.

[45] G.A.N. Connell, A.J. Lewis, "Comments on the evidence for sharp and gradual optical absorption edges in amorphous germanium." Physica status solidi (b) 60.1 (1973): 291-298.

[46] H. F. Cordes, "Preexponential factors for solid-state thermal decomposition. The Journal of Physical Chemistry, 72(6)) 1968) 2185-2189.

[47] J. Tauc, "Amorphous and Liquid Semiconductors", Springer Science & Business Media, 2012.

[48] A.A. Akl, H. Kamal, K. Abdel-Hady, "Fabrication and characterization of sputtered titanium dioxide films", Applied Surface Science, 252 (2006) 8651–8656.

[49] S.I. Cordoba-Torresi, A. Hugot-Le Goff, S. Joiret "Electrochromic behavior of nickel oxide electrodes: ii. identification of the bleached state by Raman spectroscopy and nuclear reactions." Journal of the Electrochemical Society 138.6 (1991): 1554.

[50] N.F. Mott, E.A. Davis, Electronic Processes in Non-Crystalline Materials, Clarendon, Oxford, (1979).

[51] S. Hasegawa and M. Kitagawa "Effects of annealing on localized states in amorphous Ge films". Solid State Communications, 27(9) (1978) 855-858.

[52] D. Singh, S. Kumar, R. Thangaraj, T. Sathiaraj, "Influence of thickness on optical properties of a-$(Se_{80}Te_{20})_{96}Ag_4$ thin films", Physica B: Condensed Matter, 408 (2013) 119-125.

[53] R. Achour, B. Said, B. Boubaker, "The effect of the film thickness and doping content of SnO2:F thin films prepared by the ultrasonic spray method", Journal of Semiconductors, 34 (2013) 093003.

[54] M.A. Abdel-Rahim, M.M. Hafiz, A.Z. Mahmoud, "Influence of thickness and annealing on optical constants of $Se_{82.5}Te_{15}Sb_{2.5}$ chalcogenide thin films", Solid State Sciences, 48 (2015) 125-132.

International Current Journal of Engineering and Science (ICJES)
Volume 4, Issue 11, pp 55-86, November-2025
ISSN (Online): 2583-7257
Article DOI: https://doi.org/10.47001/ICJES/2025.411010

[55] M. El-Hagary, M. Emam-Ismail, E. Shaaban, A. Al-Rashidi, S. Althoyaib, "Composition, annealing and thickness dependence of structural and optical studies on $Zn_{1-x}Mn_xS$ nanocrystalline semiconductor thin films", Materials Chemistry and Physics, 132(2-3), 581-590.
[56] Mansour Mohamed, E.R. Shaaban, Mohamed N. Abd-el Salam, A.Y. Abdel-Latief, Safwat A. Mahmoudd, M.A. Abdel-Rahima, "Investigation of the optical and electrical parameters of $As_{47.5}Se_{47.5}Ag_5$ thin films with different thicknesses for optoelectronic applications" Optik - International Journal for Light and Electron Optics 178 (2019) 1302–1312
[57] Florin Abeles (Ed.), Optical Properties of Solids, vol. 138, North-Holland, Amsterdam, 1972.
[58] Pankaj Sharma, S.C. Katyal, "Linear and nonlinear refractive index of As–Se–Ge and Bi doped As–Se–Ge thin films", J. Appl. Phys. 107 (2010) 113527, 11.
[59] Charles C. Wang, "Empirical relation between the linear and the third-order nonlinear optical susceptibilities", Phys. Rev. B 2.6 (1970) 2045.
[60] L. Liu, T. Cheng, K. Nagasaka, H. Tong, G. Qin, T. Suzuki, Y. Ohishi, "Coherent midinfrared supercontinuum generation in all-solid chalcogenide microstructured fibers with all-normal dispersion", Opt. Lett. 41 (2016) 392-395.
[61] N.L. Boling, A. Glass, A. Owyoung, "Empirical relationships for predicting nonlinear refractive index changes in optical solids", IEEE J. Quant. Electron. 14 (1987) 601–608.
[62] J.C. Phillips, Bonds and Bands in Semiconductors, Academic Press, New York and London, 1973.
[63] V. Kumar, B.S.R. Sastry, "Heat of formation of ternary chalcopyrite semiconductors", J. Phys. Chem. Solid. 66 (1) (2005) 99–102.
[64] V.P. Gupta, V.K. Srivastava, P.N.L. Gupta, "Electronic properties of chalcopyrites", J. Phys. Chem. Solid. 42 (12) (1981) 1079–1085.
[65] M.M. El-Nahass, A.A.M. Farag, "Structural, optical and dispersion characteristics of nanocrystalline GaN films prepared by MOVPE", Optic Laser. Technol. 44 (2) (2012) 497–503.
[66] R.R. Reddy, Y. Nazeer Ahammed, K. Rama Gopal, P. Abdul Azeem, T.V.R. Rao, P. Mallikarjuna Reddy, "Optical electronegativity, bulk modulus and electronic polarizability of materials", Opt. Mater. 14 (4) (2000) 355–358.
[67] Ahmed Saeed Hassanien, Ishu Sharma, A. Alaa, Akl. "Physical and optical properties of a-Ge-Sb-Se-Te bulk and film samples: refractive index and its association with electronic polarizability of thermally evaporated a-$Ge_{15-x}Sb_xSe_{50}Te_{35}$ thin-films, J. Non-Cryst. Solids 531 (2020) 119853.
[68] J.A. Duffy, "Trends in energy gaps of binary compounds: an approach based upon electron transfer parameters from optical spectroscopy", J. Phys. C Solid State Phys. 13 (16) (1980) 2979.
[69] Ahmed Saeed Hassanien, "Studies on dielectric properties, optoelectrical parameters and electronic polarizability of thermally evaporated amorphous $Cd_{50}S_{50-x}Se_x$ thin films", J. Alloys Compd. 671 (2016) 566–578.
[70] S.K. Tripathy, "Refractive indices of semiconductors from energy gaps", Opt. Mater. 46 (2015) 240–246.
[71] T.S. Moss, "A relationship between the refractive index and the infra-red threshold of sensitivity forphotoconductors", Proc. Phys. Soc. B 63 (1950) 167.
[72] N.M. Ravindra, Sushil Auluck, V.K. Srivastava, "On the Penn gap in semiconductors", Phys. Status Solidi 93 (1979) K155–K160
[73] P. Herve, L.K.J. Vandamme, "General relation between refractive index and energy gap in semiconductors", Infrared Phys. Technol. 35 (1994) 609–615.
[74] P.J.L. Herve, L.K.J. Vandamme, "Empirical temperature dependence of the refractive index of semiconductors", J. Appl. Phys. 77 (1995) 5476–5477.
[75] R.R. Reddy, S. Anjaneyulu, C.L.N. Sarma, "Relationship between energy gap, refractive index, bond energy and the szigeti charge in polyatomic binary compounds and semiconductors", J. Phys. Chem. Solid. 54 (1993) 635–637.
[76] V.P. Gupta, N.M. Ravindra, "Comments on the moss formula", physica status solidi (b) 100 2 (1980) 715–719.

****

